Journal of
Vibration and Control

Feedback Control of LCOs and Transonic buzz, using the Nonlinear TSD Aerodynamics

Journal:	*Journal of Vibration and Control*
Manuscript ID	JVC-21-0396.R1
Manuscript Type:	Original Manuscript
Date Submitted by the Author:	n/a
Complete List of Authors:	Kwon, Jae; Aerospace Technology Research Institute, Agency for Defense Development Vepa, Ranjan; Queen Mary, University of London, United Kingdom, School of Engineering and Materials Science
Keywords:	Transonic buzz, Buffeting, Limit cycle oscillator, Feedback control, Transonic small-disturbance theory
Please select up to 5 subject areas that best reflect the content of your manuscript:	Fundamental dynamics,Modeling, Aeroelasticity, Non-linear dynamics , Control theory, Analytical methods
Abstract:	In this paper a systematic method to suppress transonic buzz with feedback is presented. A trailing edge control surface in the form of part-span flap was used only to modify and control the unsteady aerodynamic loading on the wing. The flap rotation was used to provide feedback, which consisted of a weighted linear combination of the amplitudes of the principal modes of the structure, referred to as the control law. A linear, optimal feedback control law, that is synthesised systematically based on pseudo-spectral time domain analysis, may be used in principle, to assess its capacity to actively suppress the buzz in the transonic flow domain by using a servo-controlled control surface to modify the unsteady, nonlinear aerodynamic loads on the wing. Thus it is essential that a set of feasible control laws are first constructed. In this paper, this is done by applying the doublet-lattice method (DLM). Restrictions, such as near-zero structural damping in the flap mode, were imposed on the aeroelastic model to facilitate the occurrence of transonic buzz. The feasible set of control laws were then assessed using the nonlinear transonic small disturbance (TSD) theory and an optimum control is selected to suppress the buzz. The essential difference of the behaviour of the closed loop system in non-linear transonic flow, when compared to the applications of linear optimal control in linear potential flow, are presented and discussed.

Feedback Control of LCOs and Transonic buzz, using the Nonlinear TSD Aerodynamics

Jae Ryong Kwon,

Aerospace Technology Research Institute, Agency for Defense Development,

Daejeon, 34186, Republic of Korea.

Ranjan Vepa,

School of Engineering and Material Science, Queen Mary, University of London,

London, E14NS, UK.

ABSTRACT

In this paper a systematic method to suppress transonic buzz with feedback is presented. A trailing edge control surface in the form of part-span flap was used only to modify and control the unsteady aerodynamic loading on the wing. The flap rotation was used to provide feedback, which consisted of a weighted linear combination of the amplitudes of the principal modes of the structure, referred to as the control law. A linear, optimal feedback control law, that is synthesised systematically based on pseudo-spectral time domain analysis, may be used in principle, to assess its capacity to actively suppress the buzz in the transonic flow domain by using a servo-controlled control surface to modify the unsteady, nonlinear aerodynamic loads on the wing. Thus it is essential that a set of feasible control laws are first constructed. In this paper, this is done by applying the doublet-lattice method (DLM). Restrictions, such as near-zero structural damping in the flap mode, were imposed on the aeroelastic model to facilitate the occurrence of transonic buzz. The feasible set of control laws were then assessed using the nonlinear transonic small disturbance (TSD) theory and an optimum control is selected to suppress the buzz. The essential difference of the behaviour of the closed loop system in non-linear transonic flow, when compared to the applications of linear optimal control in linear potential flow, are presented and discussed.

Keywords: Transonic buzz, Buffeting, Limit cycle oscillator, Feedback control, Transonic small-disturbance theory.

1. Introduction

There are two classes of aeroelastic instabilities driven by aerodynamic non-linearities, which are commonly referred to as buffet and control surface buzz. Oscillations induced in the aircraft lifting or control surfaces due to the presence of a turbulent wake or under the influence of vortex flows are generally referred to as buffeting. Control surface buzz is a sustained aeroelastic oscillation which is a particular type of Limit Cycle Oscillation (LCO) and is observed on trailing edge control surfaces. The continuous interaction of the shocks with a boundary layer especially over a control surface results in the oscillation of the control surface and is known as a buzz. Lambourne (1964) and Bendiksen (1993) provided the earliest classifications of transonic buzz. Rampurawala (2005) has provided an excellent discussion of the existence of buzz in several real aircraft and also considered the prediction of buzz using computation fluid dynamics based analysis techniques. Timme and Badcock (2009) and Woodgate and Badcock (2009) have discussed the application of techniques such the higher order harmonic balance methods to the prediction of transonic buzz. Greco Jr. and Lan (2010) have applied the nonlinear TSD theory to the problem of buzz prediction in the frequency domain rather than in the time domain. Edwards (2010) was able to predict the onset of buffet and the existence of LCOs at transonic speeds. In earlier reviews Dowell and Hall (1996), Dowell, Edwards and Strgnac (2003) and Dowell (2010) have covered the past developments in the prediction of transonic buzz.

The use of high-fidelity methods to obtain the transonic buzz boundaries can be computationally expensive. Considering a typical set of the three-dimensional unsteady Euler equations in conservative differential form and in curvilinear coordinates the state vector is defined by the conservative flow variables vector. The flow variables vector, in its simplest form is at least five dimensional, consisting of the density, flow momentum in three Cartesian directions and the energy. Given the amount of computational time required to perform high-fidelity fluid-structure interaction analyses using the five-dimensional Euler equations over a computational grid spanning the flow field, the model orders are reduced by introducing relevant reduction techniques such as Proper Orthogonal Decomposition (POD) or Polynomial Chaos Expansion. When a reduced order model is adopted, the number of flow variables over the entire flow field are also generally reduced. These computations

must be repeated several times in order to study the oscillatory behaviour under transonic flow conditions. Comparing with the Nonlinear TSD methodology, where one is using only a two-dimensional set of flow variables, the computational cost is reduced substantially, even when reduced order modelling is adopted. Greco Jr. and Lan (2010), Im, Kim and Choi (2018), Shukla and Patil (2017), Howison et al (2018), Taddei (2021), Vuong, Kim and Dinh, (2021), Li and Ekiki (2019), Munk et al (2020), He et al (2019), Prasad (2020) and Prasad and Choi (2020) while Yang et al (2020) used various reduced order models to predict transonic buzz.

Considering the active feedback control of transonic buzz there have been a few attempts to systematically study the effects of feedback on transonic buzz. Verstraelen, Kerschen, Dimitriadis (2017) have attempted to suppress transonic buzz using dynamic vibration absorbers. Marzocca, Silva and Librescu (2002) have alos considered the closed loop analysis of transonic buzz. Goa et al (2017) have considered the analysis of transonic buffet with active controls.

The primary focus of this paper is the suppression of transonic buzz by the use of feedback control. In this paper a systematic, computational model based method to suppress transonic buzz with feedback is presented. There are several unsteady mechanisms in transonic flow, including transonic buzz, pre-buffet flow and transonic buffet onset, forced vibration of aerofoil motion and buffeting response and unstable transonic buffet flow. Although different qualitative interpretation of transonic buzz exist, two conditions must be present for transonic buzz type LCOs to persist. First the linear dynamics of the flap must be in a near state of simple harmonic oscillations. Secondly the nonlinear perturbations to the dynamics due to shock wave motions, boundary layer separation and related transonic phenomenon must be able to sustain the limit cycle oscillations in the single-degree of freedom system. If either of these two conditions are not present, transonic buzz would be inhibited. In this paper, a linear feedback control law is synthesized, so that the first condition is not met. Thus a basic principle for the synthesis of a control law to suppress transonic buzz was established based on the pseudo-spectral time domain analysis of LCOs.

In this paper, furthermore, a trailing edge control surface was used to provide full state feedback. Given a feedback control law, it is possible in principle, to assess its capacity to actively suppress the buzz in the transonic flow domain by using a servo-controlled control surface to modify the unsteady aerodynamic loads on the wing. Thus it is essential that a set of feasible linear control laws are first constructed

by applying the doublet-lattice method (DLM) as was successfully implemented earlier by Vepa and Kwon (2021) for the active suppression of transonic flutter. In this paper the methodology is modified, so the modes of buzz oscillations can be controlled. Restrictions, such as near-zero structural damping in the flap mode, were imposed on the aeroelastic model to facilitate the occurrence of transonic buzz. This aspect is explained in the section 3, after reviewing the analysis of LCOs in section 2. The buzz prediction methodology is discussed in section 4 and the assessment and the selection of an optimum control law to suppress the buzz is considered in section 5. A typical example is considered and the results are presented in sections 6.

2. Analysis of Limit Cycle Oscillators

First the fascinating subject of the analysis of LCOs will be briefly revisited. The Poincaré-Bendixson theorems can be used to identify the presence and absence of limit cycles and establish their uniqueness. These important theorems are explained and are briefly summarized in Vepa (2016). As a result of the Poincaré-Bendixson theorems (see for example Vepa, 2016), in the case of the following second-order equation,

$$\ddot{x} + g(x)\dot{x} + f(x) = 0\,, \tag{1}$$

where, x is a displacement, $f(x)$ and $g(x)$ are nonlinear functions of x and the dot over the variable $(\dot{x})$ represents differentiation with respect to time t. One may state without proof, that it has a periodic solution which is unique and that this solution is an asymptotically stable orbit under a given set of conditions.

To present the gist of the method of variation of parameters, consider a non-linear system with governing equation of motion expressed as,

$$\ddot{x}(t) + x(t) + \varepsilon\, F(\dot{x}, x) = 0\,, \tag{2a}$$

subject to the initial conditions,

$$x(t)\big|_{t=0} = a_0\,,\ \dot{x}(t)\big|_{t=0} = 0\,, \tag{2b}$$

where $x(t)$ is the displacement, $F(\dot{x}, x)$ is a non-linear function, ε is a small non-linearity or perturbation parameter and a_0 is a constant. When ε is set equal to zero the solution is of the form,

$$x(t) = a_0 \cos(t + \phi)\,. \tag{3}$$

Hence, when the perturbation parameter ε is not equal to zero the solutions for the displacement and velocity are assumed to be of the form,

$$x(t) = a(t)\cos(t + \phi(t)),\ \dot{x}(t) = -a(t)\sin(t + \phi(t)) \tag{4}$$

where $a(t)$ is a time dependent slowly varying amplitude function and $\phi(t)$ is again a time dependent and slowly varying phase angle, relative to a vector rotating in the phase plane with a constant angular velocity.

Differentiating the assumed solutions and solving for $\dot{a}(t)$ and $\dot{\phi}(t)$, one obtains,

$$\dot{a}(t) = \varepsilon\, F(-a\sin\psi, a\cos\psi)\sin\psi\,, \tag{5a}$$

$$\dot{\phi}(t) = \varepsilon\, F(-a\sin\psi, a\cos\psi)\cos\psi \tag{5b}$$

where, $\psi = t + \phi(t)$, is the phase angle of the amplitude vector relative to its initial direction. The approximation, known as the *Krylov-Bogoliubov averaging* is introduced by replacing the periodic terms in the right hand sides of the above equations for $\dot{a}(t)$ and $\dot{\phi}(t)$, by their averages over one period of oscillation; i.e. $\psi = 0$ to $\psi = 2\pi$. Further both $a(t)$ and $\phi(t)$ are assumed to be constant over the integration period. Without any loss of generality, the averaged equations take the form,

$$\dot{a}(t) = \varepsilon\, f_{KB}(a),\ \dot{\phi}(t) = \varepsilon\, g_{KB}(a). \tag{6}$$

The response and stability of the slowly varying amplitude function is determined by the first of these averaged equations (6) while the phase angle is the obtained from the second. Orthogonal series expansion in the amplitude and phase plane in terms of ultra-spherical polynomials also leads to equations similar to equations (6).

The method of analysis was first postulated by Denman (1964) and developed by several others. Caughey and Payne (1969) have also considered a similar class of oscillators with stochastic excitation.

Expanding the right hand sides of the equations for the amplitude, $a(t)$ and phase $\phi(t)$ in terms of the variable z, in an orthogonal series of ultra-spherical polynomials with parameter λ and retaining only the first term, one has the approximations,

$$\dot{a}(t) = \varepsilon\, f_U(a, \lambda),\ \dot{\phi}(t) = \varepsilon\, g_U(a, \lambda), \tag{7}$$

as the polynomial, $P_0^{\lambda}(z)$ is a constant. In particular when $\lambda = 1/2$,

$$\dot{a}(t) = \varepsilon f_U(a,\lambda)\big|_{\lambda=\frac{1}{2}} = \varepsilon f_{KB}(a), \tag{8a}$$

$$\dot{\phi}(t) = \varepsilon g_U(a,\lambda)\big|_{\lambda=\frac{1}{2}} = \varepsilon g_{KB}(a). \tag{8b}$$

Thus the averaging technique may be interpreted as a generalised orthogonal series expansion based approximation of the equations governing the dynamics in the amplitude and phase plane.

3. Principles of Control Law Synthesis for suppression of LCOs

Following the discussion in the preceding section, to synthesize a controller, since the system behaves like a periodic system as it approaches the limit cycle, and from equations (8), $\dot{a}(t) = \varepsilon f_U(a,\lambda)\,;\,0$ and $\dot{\phi}(t) = \varepsilon g_U(a,\lambda)\,;\,0$. Thus it is possible to set, $\varepsilon = 0$ and from equation (5a), one has,

$$\ddot{x}(t) + x(t) + \varepsilon F(\dot{x}, x)\,;\ \ddot{x}(t) + x(t)\,;\ 0. \tag{9}$$

In first order form, with the inclusion of a control input u,

$$\frac{d}{dt}\begin{bmatrix} x \\ \dot{x} \end{bmatrix} = \begin{bmatrix} 0 & 1 \\ -1 & 0 \end{bmatrix}\begin{bmatrix} x \\ \dot{x} \end{bmatrix} + \begin{bmatrix} 0 \\ 1 \end{bmatrix} u. \tag{10}$$

If one wishes to design a steady state feedback regulator that minimizes the performance index,

$$J = \int_0^\infty \left(x^2 + \dot{x}^2\right) dt. \tag{11}$$

An algebraic Riccati equation must be solved and it can be shown that,

$$u = -\begin{bmatrix} k_1 & k_2 \end{bmatrix}\begin{bmatrix} x & \dot{x} \end{bmatrix}^T = -\begin{bmatrix} 0.4142 & 1.3522 \end{bmatrix}\begin{bmatrix} x & \dot{x} \end{bmatrix}^T. \tag{12}$$

The above control input based on the linear-quadratic regulator theory, is independent of $F(\dot{x}, x)$. A simple example will illustrate the open and closed loop responses of a typical oscillator.

The typical example considered is the modified van der Pol equation with parameters $\mathbf{b} = [b_i]$ which may be expressed as,

$$\ddot{x}(t) + x(t) - \left(b_1\left(1 - x^2\right) + b_2\left(1 - \dot{x}^2\right) + b_3\left(1 - x^2 - \dot{x}^2\right) + b_4\left(1 - x^4\right)\right)\dot{x}(t) = u \tag{13}$$

Ignoring the control input, the equations corresponding to (5a) and to (5b) may be respective expressed as,

$$\dot{a}(t) = a(t)\sum_{n=1}^{3} f_{nb}\left(\frac{1-\cos 2n\psi}{2^n}\right),\ \dot{\phi}(t) = \varepsilon\sum_{n=1}^{3} g_{nb}\left(\frac{\sin 2n\psi}{2^n}\right) \tag{14a}$$

where, the functions f_{nb} and g_{nb} may be expressed in terms of amplitude $a(t)$ as,

$$\begin{bmatrix} f_{1b} \\ f_{2b} \\ f_{3b} \end{bmatrix} = \begin{bmatrix} 1 & 1-a^2 & 1-a^2 & 1-a^4/16 \\ -a^2/2 & a^2/2 & 0 & a^4/4 \\ 0 & 0 & 0 & a^4/4 \end{bmatrix} \begin{bmatrix} b_1 \\ b_2 \\ b_3 \\ b_4 \end{bmatrix} \tag{14b}$$

and

$$\begin{bmatrix} g_{1b} \\ g_{2b} \\ g_{3b} \end{bmatrix} = \begin{bmatrix} 1-a^2/2 & 1-a^2/2 & 1-3a^2/2 & 1-5a^4/8 \\ a^2/2 & -a^2/2 & 0 & -a^4 \\ 0 & 0 & 0 & a^4/2 \end{bmatrix} \begin{bmatrix} b_1 \\ b_2 \\ b_3 \\ b_4 \end{bmatrix}. \tag{14c}$$

Expanding $\cos 2n\psi$ and $\sin 2n\psi$ in terms of ultra-spherical polynomials in the interval $[0, 2\pi]$ and retaining only the first term in the orthogonal series expansion, the equations corresponding to equations (7) may be expressed as,

$$\dot{a}(t) = a(t)\sum_{n=1}^{4} b_n f_n(a)\ ,\ \dot{\phi}(t) = 0 \tag{15a}$$

where,

$$\begin{bmatrix} f_1 \\ f_2 \\ f_3 \\ f_4 \end{bmatrix} = \frac{1-U_2}{2}\begin{bmatrix} 1 \\ 1 \\ 1 \\ 1 \end{bmatrix} + \frac{a^2}{8}\begin{bmatrix} 1 & 0 & -1 & 0 \\ 3 & -4 & 1 & 0 \\ 4 & -4 & 0 & 0 \\ 0 & 0 & 0 & 0 \end{bmatrix}\begin{bmatrix} 1 \\ U_2 \\ U_4 \\ U_6 \end{bmatrix} + \frac{a^4}{16}\begin{bmatrix} 0 & 0 & 0 & 0 \\ 0 & 0 & 0 & 0 \\ 0 & 0 & 0 & 0 \\ 2 & 1 & -2 & -1 \end{bmatrix}\begin{bmatrix} 1 \\ U_2 \\ U_4 \\ U_6 \end{bmatrix} \tag{15b}$$

and

$$U_k = \Gamma(\lambda+1)J_\lambda(k\pi)/(k\pi/2)^\lambda\ . \tag{15c}$$

The parameter λ is chosen to be equal to 2 but similar results were obtained for several other choices such that $0 \le \lambda \le 9/2$. The LCO behaviour can be verified by solving equations (15) and plotting the phase-plane trajectory.

A typical set of limit cycle oscillator responses are also generated by simulating equation (13) with the additional control input given by equation (12) and with the parameter set,

$$\mathbf{b} = [0 \quad 0 \quad 0 \quad 1]. \tag{16}$$

The limit cycle responses obtained for the simulated limit cycle oscillator with $\mathbf{b}$ given by equation (16) and with and without the control input are compared in figure 1. Also shown is the closed loop response for the initially assumed alternate parameter set, $\mathbf{b}$ given by equation (17),

$$\mathbf{b} = \begin{bmatrix} 1 & 0 & 0 & 0 \end{bmatrix}. \tag{17}$$

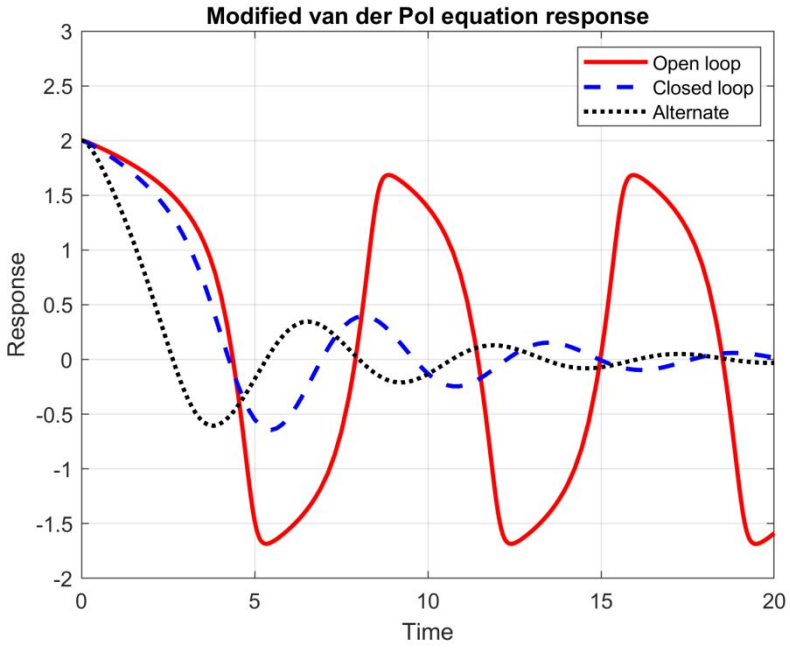

Fig. 1 Comparison of the limit cycle oscillator responses with $\mathbf{b}$ given by equation (16) and closed loop responses with $\mathbf{b}$ given by equations (16) and (17).

The principle established in the preceding equations will be applied to the problem of controlling transonic buzz.

4. Prediction of Transonic buzz

In general three-dimensional flow, the unsteady equation for the potential function ϕ, may be written in conservation form as,

$$\frac{\partial f_0}{\partial \tau} + \frac{\partial f_1}{\partial x^*} + \frac{\partial f_2}{\partial y^*} + \frac{\partial f_3}{\partial z^*} = 0, \tag{18}$$

where the functions f_i are functions of the partial derivatives of ϕ given by,

$$f_0 = -M^2\left(\phi_\tau + 2\phi_{x^*}\right), \quad f_1 = \left(1 - M^2\right)\phi_{x^*} + F\phi_{x^*}^2 + G\phi_{y^*}^2, \quad f_2 = \phi_{y^*} + H\phi_{x^*}\phi_{y^*},$$

$$f_3 = \phi_{z^*}. \tag{19}$$

In the equations (19), the coefficients F, G, and H are respectively given by,

$$F=-(\gamma+1)M^2/2,\ G=(\gamma-3)M^2/2,\ H=-(\gamma-1)M^2. \tag{20}$$

where $M=M_\infty$, is the free stream Mach number. Furthermore,

$$x^*=x/c_r,\ y^*=y/c_r,\ z^*=z/c_r,\ \tau=tU_\infty/c_r. \tag{21}$$

There are alternate coefficients that could be used for the coefficients F, G, and H.

	subsonic	supersonic
Far upstream	$\phi=0$	$\phi=0$
Far downstream	$C\phi_t+\phi_x=0$	$\phi_x=0$
Far above	$D\phi_t+\phi_z=0$	$\beta\phi_t+\phi_z=0$
Far below	$D\phi_t-\phi_z=0$	$\beta\phi_t-\phi_z=0$
Far spanwise	$D\phi_t+\phi_y=0$	$\beta\phi_t+\phi_y=0$
Symmetry plane	$\phi_y=0$	$\phi_y=0$

Table I The applicable boundary conditions

The applicable boundary conditions are summarised in Table I. In Table I, the coefficients β, D and C, are given by,

$$\beta=\sqrt{M^2-1},\ D=M\sqrt{1+M^2/(2F\phi_x-\beta^2)},$$
$$C=\left(D\sqrt{(2F\phi_x-\beta^2)}-M^2\right)/(2F\phi_x-\beta^2). \tag{22}$$

The streamwise flux is a major component in the potential equation and is,

$$f_1=(1-M^2)\phi_{x^*}+F\phi_{x^*}^2+G\phi_{y^*}^2. \tag{23}$$

An efficient three-dimensional aerodynamic code based on the nonlinear TSD theory was developed by Batina (1988, 1989, 1992) and later improved by Kim et al (2005) and by Kwon, Yoo and Lee (2018).

Generally, given a reference length such as the root chord c_r, the free stream density ρ_∞ and the free stream flow velocity U_∞, one can construct the generalized aerodynamic forces matrix $\mathbf{Q}$ defined by,

$$\mathbf{Q}=\tfrac{1}{2}\rho_\infty U_\infty^2 c_r^3 \int_{S^*}\left(z_i(x^*,y^*)/c_r\right)\Delta C_{p,j}\left((z_j/c_r),x^*,y^*,M_\infty\right)dS^*, \tag{24}$$

where z_j is the vibration mode shape function of the structure in the j^{th} mode, S^* is the non-dimensional planform area, x^* and y^* are the non-dimensional coordinates of a point in the planform, and M_∞ is the free stream Mach number, the ratio of the free stream flow velocity to the local speed of sound. Furthermore $\Delta C_{p,j}\left(\left(z_j/c_r\right), x^*, y^*, M_\infty\right)$ is the unsteady pressure distribution on the wing surface induced by the j^{th} modal displacement.

The equations of motion of the vibrating wing, including the partial-span trailing edge flap, take the form,

$$\mathbf{M}\ddot{\mathbf{q}} + \mathbf{C}\dot{\mathbf{q}} + \mathbf{K}\mathbf{q} = \mathbf{Q}_{tsd}\left(\mathbf{q}, \dot{\mathbf{q}}, M_\infty\right) + \mathbf{Q}_{tsd,\eta}\left(\mathbf{q}, \dot{\mathbf{q}}, M_\infty\right)\eta\,, \tag{25}$$

where the vectors $\mathbf{Q}_{tsd}\left(\mathbf{q}, \dot{\mathbf{q}}, M_\infty\right)$ and $\mathbf{Q}_{tsd,\eta}\left(\mathbf{q}, \dot{\mathbf{q}}, M_\infty\right)$ are obtained using a code based on the nonlinear TSD formulation. The integration of the equations (25) is done by a time-marching method, with the appropriate initial conditions as described by Kwon, Kim and Lee (2004) and is the basis of the coupled time integration method (CTIM). In the frequency domain, with all the initial conditions set to zero, a pulse input is used to generate the response as in the transient pulse method (PM), described by Kwon, Kim and Lee (2004).

5. Control Law Synthesis for the Suppression of Transonic Buzz

In the equation (24) for the generalized aerodynamic forces matrix, the integration is performed over the planform area. The modal displacements and slopes at the sending and receiving points in the Doublet Lattice Method (DLM) code are obtained by spline interpolation of the modal displacements at nodes of the structural model. The matrix $\mathbf{Q} = \mathbf{Q}(k)$ is generally complex and a function of the reduced frequency of oscillation, k. If one assumes a matrix Padé approximant representation, the matrix $\mathbf{Q}(k)$ may approximated as,

$$\mathbf{Q}(k) \cong \mathbf{Q}_0 + ik\mathbf{Q}_1 + \left[\mathbf{I} + ik\mathbf{Q}_p\right]^{-1}\mathbf{Q}_r\,, \tag{26}$$

where $\mathbf{Q}_0$ and $ik\mathbf{Q}_1$ are the steady state and low frequency asymptote that can be computed independently, from the steady state and low frequency asymptotes of the

subsonic kernel function as outlined by Vepa (1977). If one assumes, the augmented poles are relatively fast, which is usually the case, $\mathbf{Q}_p \approx \mathbf{0}$, and,

$$\mathbf{Q}(k) \approx \mathbf{Q}_0 + ik\mathbf{Q}_1 + \mathbf{Q}_r . \tag{27}$$

Generally the matrices $\mathbf{Q}_r$, the residue matrix and $\mathbf{Q}_p$, the matrix related to the poles corresponding to the augmented states, are constructed by matching the matrix $\mathbf{Q}(k)$ to the coefficient matrices in the matrix Padé approximant representation at some low value of the reduced frequency, $k = k_f$ close to the estimated flutter reduced frequency, and assuming k is small, it follows that,

$$\mathbf{Q}_0 + \mathbf{Q}_r \cong \mathrm{Re}\left(\mathbf{Q}(k)\right)\Big|_{k=k_f} = \mathrm{Re}\left(\mathbf{Q}\left(k_f\right)\right). \tag{28}$$

Thus $\mathbf{Q}(k)$, computed by the DLM, may be approximated by the zeroth order matrix Padé approximant and is given by,

$$\mathbf{Q}(k) \cong \mathrm{Re}\left(\mathbf{Q}\left(k_f\right)\right) + ik\mathbf{Q}_1 . \tag{29}$$

Thus given the stiffness matrix $\mathbf{K}$, of the structural system, and choosing a suitable model for the structural damping matrix $\mathbf{g}$ which is assumed to be diagonal matrix, the structural damping matrix is $\mathbf{C} = \mathbf{gK}$. The equations of motion are expressed as,

$$\mathbf{M}\ddot{\mathbf{q}} + \mathbf{C}\dot{\mathbf{q}} + \mathbf{K}\mathbf{q} = \mathrm{Re}\left(\mathbf{Q}\left(k_f\right)\right)\mathbf{q} + \left(c_r/U_\infty\right)\mathbf{Q}_1\dot{\mathbf{q}} . \tag{30}$$

or equivalently, with the flap included explicitly as,

$$\mathbf{M}\ddot{\mathbf{q}} + \mathbf{C}\dot{\mathbf{q}} + \mathbf{K}\mathbf{q} = \mathrm{Re}\left(\mathbf{Q}\left(k_f\right)\right)\begin{bmatrix}\mathbf{q} & q_\eta\end{bmatrix}^T + \left(c_r/U_\infty\right)\mathbf{Q}_1\begin{bmatrix}\dot{\mathbf{q}} & \dot{q}_\eta\end{bmatrix}^T,$$

$$\ddot{q}_\eta + 2\zeta_\eta\omega_\eta\dot{q}_\eta + \omega_\eta^2 q_\eta + \mathbf{Q}_{\mathbf{H}\eta}\left(\mathbf{q}, \dot{\mathbf{q}}, q_\eta, \dot{q}_\eta\right) = \omega_\eta^2\eta_c , \tag{31}$$

where the vector $\mathbf{q}$ does not include the flap degree of freedom, q_η is the amplitude of flap degree of freedom, η_c is the flap actuator command input, ω_η is flap actuator natural frequency, ζ_η is the flap actuator damping ratio and $\mathbf{Q}_{\mathbf{H}\eta}$ is the aerodynamic flap hinge moment. It is assumed that the damping ratio in the flap mode is zero as the

flap is in a state oscillation. The assumption is extremely important for the purpose of the synthesis of the control law.

The equations of motion defined by equations (31) may then be cast in the state space form as,

$$\dot{\mathbf{x}} = \mathbf{A}\mathbf{x} + \mathbf{B}\eta_c . \tag{32}$$

Now it is completely feasible to construct an optimal control law based on the above model formulation, defined by equation (32). The optimal control is assumed to minimize a cost function of the form,

$$J\left(\mathbf{x}(t_0), t_0\right) = \int_{t_0}^{t_f} \left(\mathbf{x}^T \mathbf{Q}_x \mathbf{x} + \mathbf{u}^T r \mathbf{R} \mathbf{u}\right) dt + \mathbf{x}^T\left(t_f\right) \mathbf{Q}_f \mathbf{x}\left(t_f\right), \tag{33}$$

where r is a scalar used to alter the control weighting matrix $\mathbf{R}$ in the formulation of the optimal control law synthesis, $\mathbf{Q}_x$ is the state vector weighting matrix and $\mathbf{Q}_f$ is the weighting matrix for the state vector at the final time $t = t_f$. For the single input case, $\mathbf{R} = 1$. The steady-state control law takes the form,

$$\eta_c = \mathbf{u} = -(1/r)\mathbf{R}^{-1}\mathbf{B}^T \mathbf{P}_\infty \mathbf{x} \equiv -\mathbf{K}_f \mathbf{x}, \ \mathbf{P}_\infty \mathbf{A} + \mathbf{A}^T \mathbf{P}_\infty + \mathbf{Q} - \mathbf{P}_\infty \mathbf{B}\mathbf{R}^{-1}\mathbf{B}^T \mathbf{P}_\infty = \mathbf{0}, \tag{34}$$

where $\mathbf{P}_\infty$ satisfies the above algebraic Riccati equation which is solved using a standard function in MATLAB.

Thus given a range of monotonically increasing free stream Mach numbers $M_{\infty,k}$, $k = 1, 2, \mathrm{L}$, as well as a set values for the relative weighting scaling parameter r, one can construct families of control laws, with differing closed-loop stability characteristics. The parameter *r*, in accordance with optimal control theory, is the ratio maximum magnitude of an element in the state vector to the maximum magnitude of the control input as explained by Vepa and Kwon (2021).

In this paper, the parameter r, provides a single scalar parameter to obtain a large distribution of control laws. Each of the control laws may then be used with the open loop dynamics, reformulated in the transonic domain based on the nonlinear TSD theory, and an optimal solution may be selected.

6. Application Example

The example considered, illustrated in figure 2, is the one considered by Kwon, Kim and Lee (2004). The model properties are summarised in Table II. The aerodynamic grid generated and used to solve for the nonlinear TSD aerodynamics is shown in Figure 3. The first three modes in the dynamic model are the first bending, the first torsion mode and the flap oscillation mode controlled by a servo-actuator, while the remaining are higher order modes.

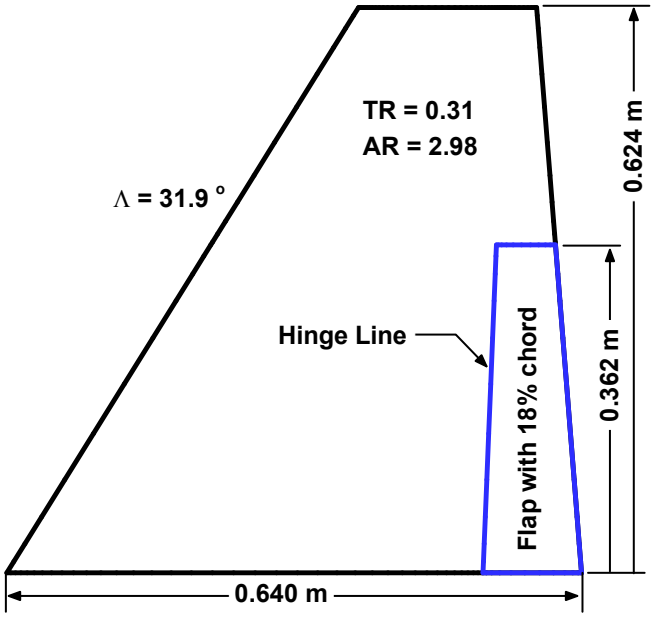

Fig.2 Planform of the application example considered (All dimensions shown are in metres.)

Hinge Stiffness, K_θ	73.4 *Nm/rad*
Flap Moment of Inertia, I_α	0.000842 kgm^2
Material Density, ρ	2770 kg/m^3
Young's Modulus, E	7.31×10^{10} *Pa*
Poisson's ratio, ν	0.33

Table II Model properties.

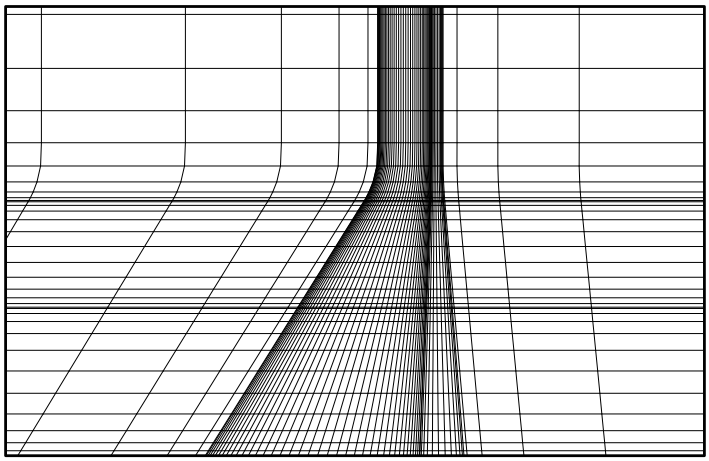

Fig. 3 Aerodynamic grid.

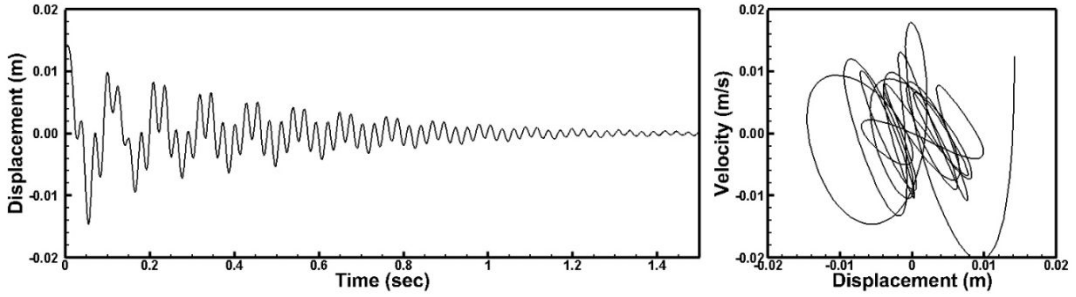

(a)

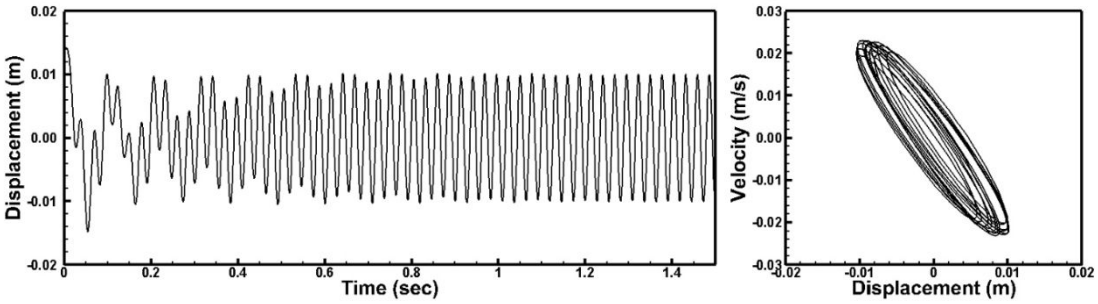

(b)

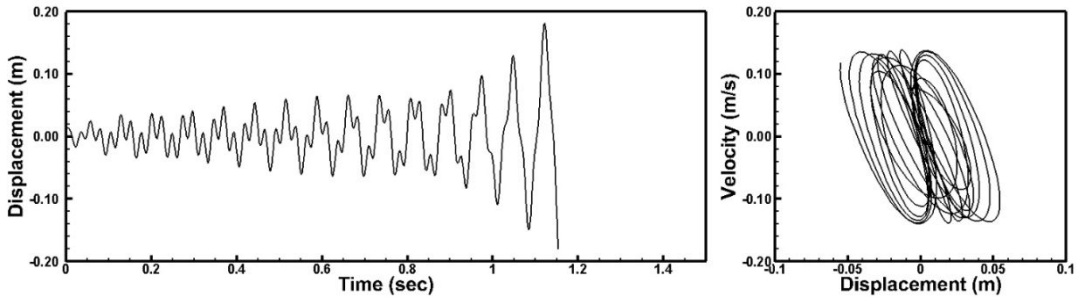

(c)

Fig. 4 Aeroelastic responses at Mach 0.95; (a) 1.49 kPa (Stable), (b) 1.67 kPa (Buzz), (c) 4.83 kPa (Unstable).

7. Typical Simulation Results

In figure 4 are shown the responses of the flap mode at 3 different values of dynamic pressure assuming the flow Mach number far upstream to be $M_\infty = 0.95$. It is seen from figure 4 (b) the response exhibits a transonic buzz type behaviour characterised by sustained periodic oscillations.

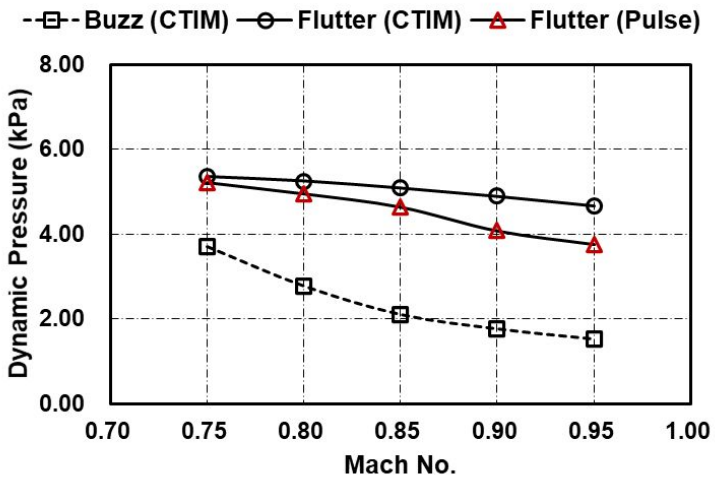

(a)

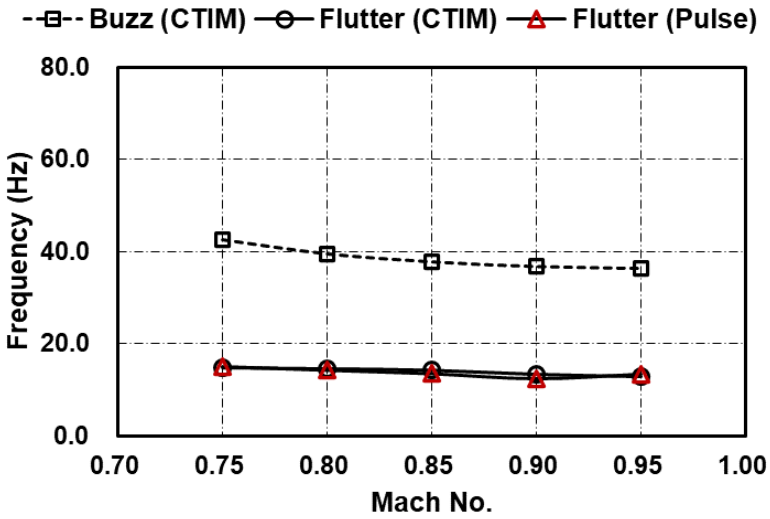

(b)

Fig. 5 Flutter and buzz boundaries with (a) dynamic pressure, (b) frequency versus Mach number.

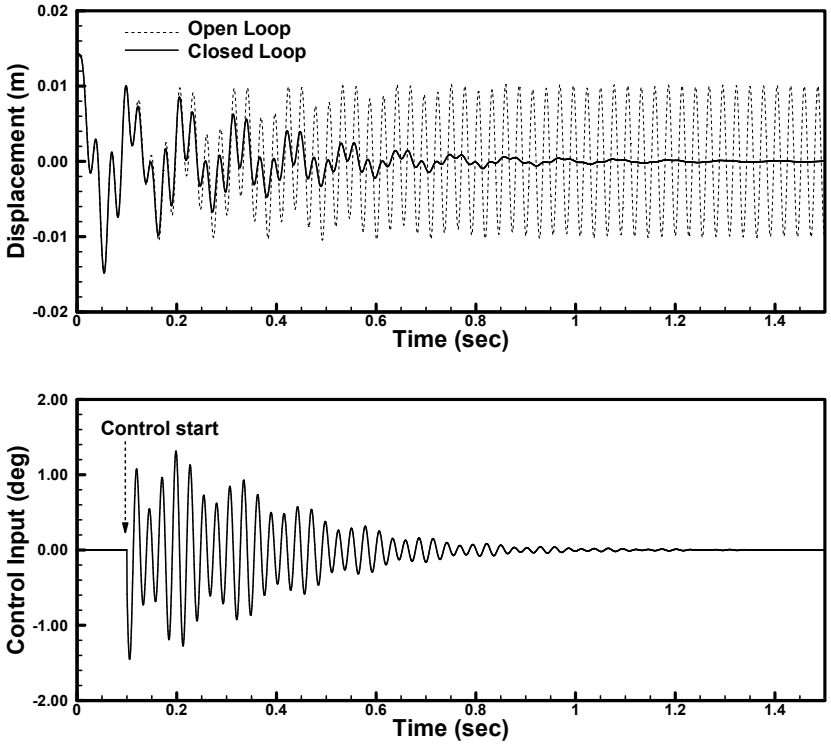

Fig. 6 Typical open and closed loop transonic buzz responses at Mach 0.95 and $q_\infty = 1.67$ kPa as well as the control input time history.

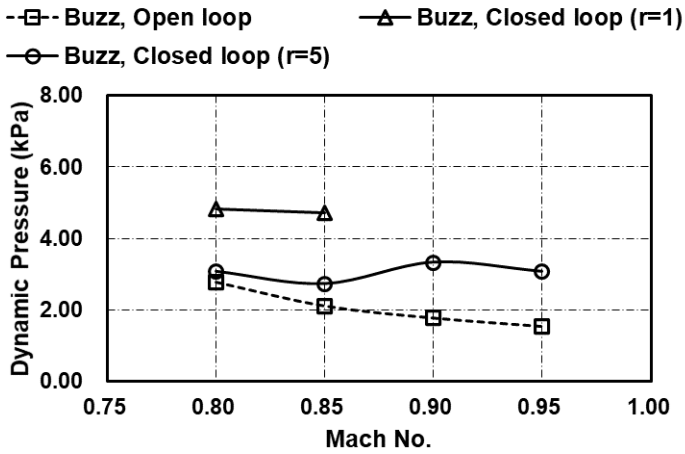

(a)

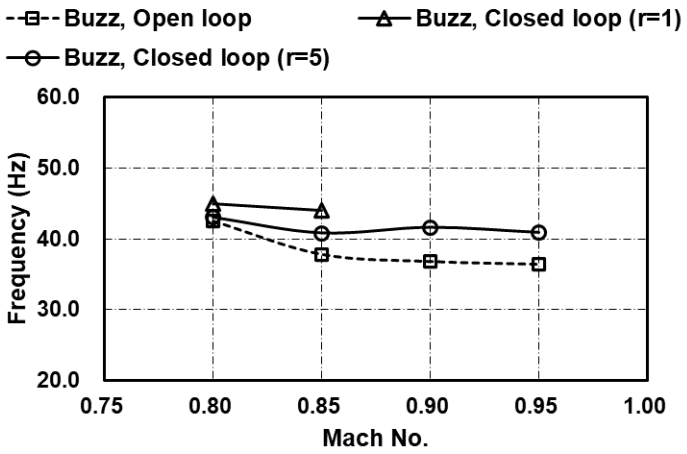

(b)

Fig. 7 Open and closed loop transonic buzz boundaries: (a) dynamic pressures at the boundary and (b) frequencies at the boundary.

The corresponding transonic flutter and buzz boundaries are compared in figure 5. The computations were done by the DLM and the coupled time integration method (CTIM) in the time domain and by the transient pulse method (Pulse) in the frequency domain, for one case, as a check. A single degree of freedom instability associated with the flap mode was observed at a similar set of Mach numbers. These results were used to synthesize the control laws and for r values, in equations (33) and (34), ranging from 1 to 200, in steps of 10 and for 6 different Mach numbers, on the buzz boundary, representing a total of 120 gain vector sets to facilitate a wide search for the optimum set of gains, as explained in sections 3 and 5.

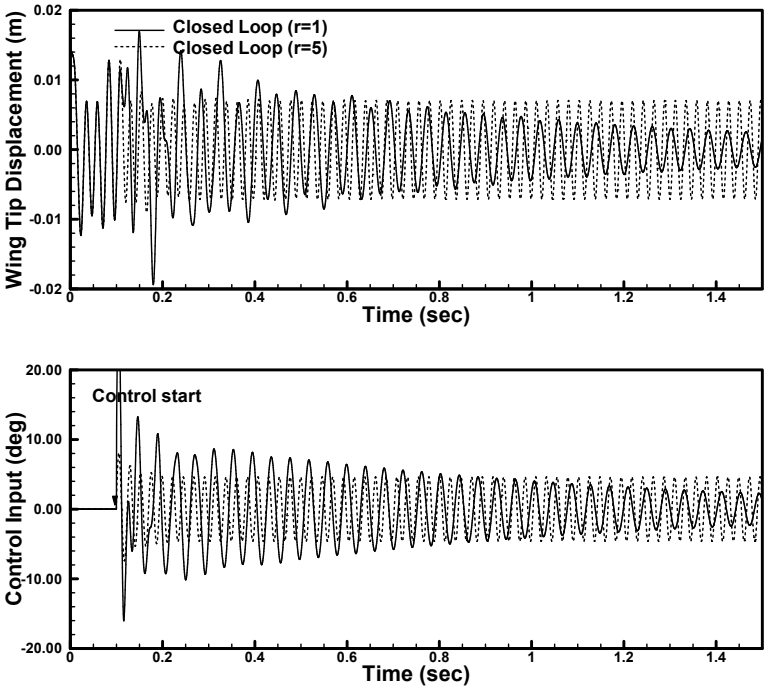

(a) Mach 0.85, $q_\infty = 3.49$ kPa

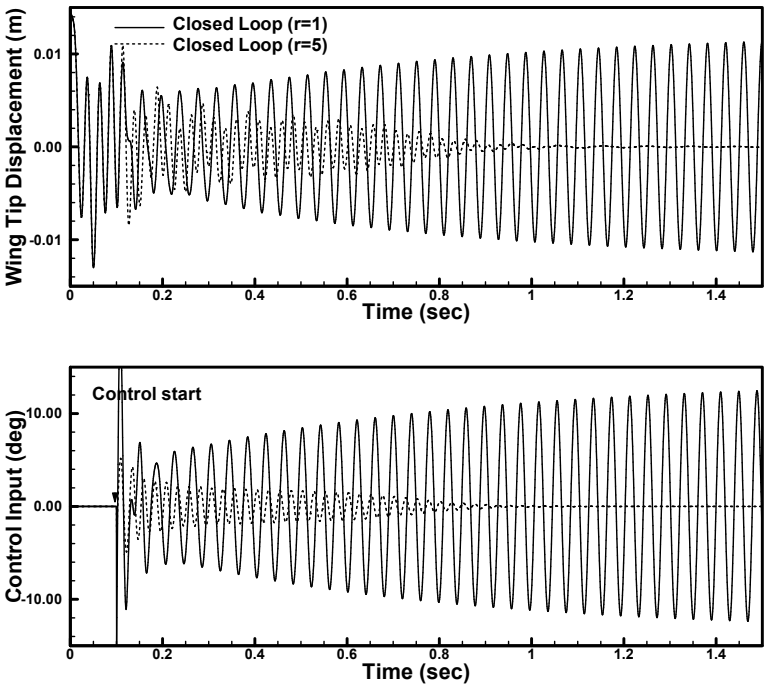

(b) Mach 0.95, $q_\infty = 2.97$ kPa

Fig. 8 Transonic buzz control response for $r = 1$ and $r = 5$ (a) Mach 0.85, $q_\infty = 3.49$ kPa and (b) Mach 0.95, $q_\infty = 2.97$ kPa.

The cases in the range of $1 \le r \le 5$, seem to provide the best control laws for maximizing the closed loop buzz velocity or buzz Mach number. In figure 6 are shown a typical set of closed loop transonic buzz responses at Mach 0.95 and $q_\infty = 1.67$ kPa as well as the control input time history. The open loop response is also shown in the background.

In figure 7 are shown a typical set of closed loop transonic buzz boundaries for $r = 1$ and $r = 5$. In the subsonic range below Mach 0.85, r values greater than 1, in the range $1 \le r \le 5$ are effective in suppressing buzz. A summary of the control parameter set applied to the simulation at Mach 0.85, is shown in Table III.

	Control gain set					
r=1	b_1	b_2	b_3	b_4	b_5	b_6
	0.0326	-4.3537	2.3285	-2.7834	0.0000	0.0000
	b_7	b_8	b_9	b_{10}	b_{11}	b_{12}
	-0.0012	0.0244	0.0860	-0.0175	0.0000	0.0000
r=5	b_1	b_2	b_3	b_4	b_5	b_6
	0.0065	-0.8745	0.4676	-0.5586	0.0000	0.0000
	b_7	b_8	b_9	b_{10}	b_{11}	b_{12}
	-0.0002	0.0049	0.0173	-0.0035	0.0000	0.0000

Table III Full state control gain set applied at Mach 0.85

However, in the transonic speed range, such as Mach 0.9 and 0.95, r values much lower than or equal to 1 are not sufficient to suppress buzz. For high Mach numbers, greater than 0.85, the computation of the closed loop buzz boundary at $r = 1$ was quite difficult due to the control surface deflection being too large for these cases, and the closed loop results tend to approach the open loop results. This feature is illustrated in figure 8, for two different r values, $r = 1$ and $r = 5$. The control surface deflection is too large, for r values below $r = 1$. Consequently the optimum range of r values is between $r = 1$ and $r = 5$.

8. Discussion and Concluding Remarks

Quite unlike linear optimal control, there is generally only a finite range of r values, over which the closed loop system is stable with the occurrence of transonic buzz effectively suppressed with reasonable magnitudes of inputs. For higher r values, the magnitude of the control input is insufficient to influence the buzz

behaviour. For lower values of the parameter r, the control inputs are very large and the nonlinear behaviour of the transonic loads is accentuated. In the subsonic range of Mach numbers, below about Mach 0.85, a small value of r is effective in suppressing the buzz. However, in the transonic range of Mach numbers, a value of r equal to or less than one is in-effective in suppressing buzz. This is because the smaller the value of r, the greater the displacement of the control surface, and the unsteady aerodynamics and consequently the wing response is sensitive to the larger displacement of the control surface in the transonic range. The small range of values of r for which the closed loop is stable, implies that for certain configurations, it may be quite impossible for the transonic buzz to be suppressed unless the control surface is designed and optimized specifically for the purpose of suppressing the transonic buzz. Control laws for suppressing transonic buzz must be selected to avoid both low and high magnitudes of control surface deflections. This is the principal contribution of this paper, apart from demonstrating the feasibility of suppressing the occurrence of transonic buzz, by the use of feedback.

Acknowledgements

The authors gratefully acknowledge the support provided by Agency for Defence Development, South Korea, through the award of a Post-Doctoral fellowship to the first author while at Queen Mary, University of London, UK, as part of the Commissioned Continuing Education programme (2019-personnel appointments (Ga)-110).

References

Batina JT (1988) Efficient algorithm for solution of the unsteady transonic small-disturbance equation. *J. of Aircraft* 25(10):962–968

Batina JT (1989) Unsteady transonic algorithm improvement for realistic aircraft applications. *J. of Aircraft* 26(2):131–139.

Batina JT (1992) A Finite-Difference Approximate-Factorization Algorithm for Solution of the Unsteady Transonic Small-Disturbance Equation, NASA Technical Paper 3129, NASA-TP-3129, 19940028359.

Bendiksen O (1993) Non-classical Aileron Buzz in Transonic Flow. 34th AIAA/ASME/ASCE/AHS/ASC Structures, Structural Dynamics and Materials Conference, AIAA paper 93–1479.

Caughey TK and Payne HJ (1967) On the response of a class of self-excited oscillators to stochastic excitation, *Int. J. Non-Linear Mech*. 2:125-151.

Denman, HH (1964) Application of Ultra-spherical Polynomials to Asymmetric Non-linear Oscillations, *J. Industrial Math. Soc*., 14(1):9-20.

Dowell EH (2010) Some recent advances in nonlinear aeroelasticity: fluid-structure interaction in the 21st century. Proceedings of the 51st AIAA/ ASME/ ASCE/ AHS/ ASC Structures, AIAA Paper no. 3137.

Dowell, EH, Edwards JW and Strganac. TW (2003) Nonlinear aeroelasticity. *Journal of Aircraft*, 40(5):857–874, ISSN 0021-8669. doi: 10.2514/2.6876. URL https://doi.org/10.2514/2.6876.

Dowell EH and Hall KC (2001) Modeling of Fluid-Structure Interaction, *Annual Reviews of Fluid Mechanics*, 33:445-490.

Edwards JW (1996) Transonic shock oscillations and wing flutter calculated with an interactive boundary layer coupling method. In 349th EUROMECH-Colloquium: Simulation of Fluid-Structure Interaction in Aeronautics, 16 - 19 Sep., 1996. URL https://ntrs.nasa.gov/search.jsp?R=19960054470.

Gao C, Zhang W, Kou J, Liu Y and Ye, Z (2017) Active control of transonic buffet flow, *J. Fluid Mech*. 824:312-351, Cambridge University Press 2017, doi:10.1017/jfm.2017.344

Greco Jr. PC and Lan CTE (2010) Frequency domain unsteady transonic aerodynamics for flutter and limit cycle oscillation prediction, *Journal of the Brazilian Society of Mechanical Sciences and Engineering*, XXXII(5), Special Issue, 434-441.

He S, Johnson E, Mader CA and Martins JRRA (2019) A Coupled Newton–Krylov Time Spectral Solver for Wing Flutter and LCO Prediction, AIAA Aviation Forum, Dallas, TX.

Howison J, Thomas J and Ekici K (2018) Aeroelastic Analysis of a wind turbine blade using the harmonic balance method, *Wind Energy*, 21(4):226-241.

Im, DK, Kim H and Choi S (2018) Mapped Chebyshev Pseudo-Spectral Method for Dynamic Aero-Elastic Problem of Limit Cycle Oscillation, *International Journal of Aeronautics and Space Sciences*, 19:316 - 329.

Kim J, Kwon H, Kim K, Lee I and Han J (2005) Numerical investigation on the aeroelastic instability of a complete aircraft model. *JSME Int. J.* Ser. B., 48(2):212–217.

Kwon H-J, Kim D-H, I. Lee I (2004) Frequency and time domain flutter computations of a wing with oscillating control surface including shock interference effects, *Aerospace Science and Technology* 8:519–532.

Kwon JR, Yoo J-H and Lee I (2018) Effects of Structural Damage and External Stores on Transonic Flutter Stability, *International Journal of Aeronautical and Space Sciences*, 19:636–644, https://doi.org/10.1007/s42405-018-0063-x.

Lambourne N (1964) Control Surface Buzz. Aircraft Research Council R & M, No. 3364.

Li H and Ekici K (2019) Aeroelastic Modelling of the AGARD 445.6 Wing Using the Harmonic-Balance-Based One-Shot Method, *AIAA Journal*, 57(11):4885-4902.

Liu YK (1965) Application of Ultra-spherical Polynomial Approximation to Non-linear Systems with Two Degrees-of-Freedom, Ph.D. dissertation, Wayne State University.

Marzocca P, Silva WA and Librescu, L (2002) Open/Closed-Loop Nonlinear Aeroelasticity for Airfoils via Volterra Series Approach, Conference Paper, 43rd AIAA/ASME/ASCE/AHS/ASC Structures, Structural Dynamics, and Materials Conference, April 2002, (also in *AIAA Journal*, (2004) 42(4):673-686.)

Munk DJ, Dooner D, Best F, Vio GA, Giannelis NF, Murray AJ and Dimitriadis G (2020) Limit cycle oscillations of cantilever rectangular wings designed using topology optimisation, Proceeding of AIAA SciTech 2020 Forum, 6-10 January 2020, Orlando, FL, USA.

Prasad R (2020) Dynamic Aeroelastic Design using Time-Spectral and Coupled Adjoint Method: Flutter/LCO Application, Doctoral dissertation submitted to the Faculty of the Virginia Polytechnic Institute and State University, Blacksburg, Virginia.

Prasad R and S. Choi S (2020) Aerodynamic Shape Optimization for Flutter/LCO based design using Coupled Adjoint, Proceedings of AIAA SciTech 2020 Forum, 6-10 January 2020, Orlando, FL, USA.

Rampurawala, AM (2005) Aeroelastic analysis of aircraft with control surfaces using CFD. PhD thesis. University of Glasgow, 2005, http://theses.gla.ac.uk/5499.

Shukla H and Patil MJ (2017) Controlling Limit Cycle Oscillation Amplitudes in Nonlinear Aeroelastic Systems, *Journal of Aircraft*, 54(5):1921 – 1932.

Taddei SR (2021) A novel blade force approach to two-dimensional mean line simulation of transonic compressor rotating stall, *Aerospace Science and Technology*, 111:106509

Timme S and Badcock KJ (2009) Oscillatory Behaviour of Transonic Aeroelastic Instability Boundaries, *AIAA Journal*, 47(6):1590-1592.

Vepa R (1977) Finite state modelling of aeroelastic system. NASA CR-2779, February 1977.

Vepa R (2016) Linear and Phase Plane Analysis of Stability, Chapter 4, in *Nonlinear Control of Robots and Unmanned Aerial Vehicles: An Integrated Approach*, CRC Press, 152-197. ISBN: 9781498767040.

Vepa R and Kwon JR (2021) Synthesis of an Active Flutter Suppression System in the Transonic Domain using a Computational Model, *The Aeronautical Journal*, To be published, 2021.

Verstraelen E, Kerschen G and Dimitriadis, G (2017) Flutter and limit cycle oscillation suppression using linear and nonlinear tuned vibration absorbers, *Shock & Vibration, Aircraft/Aerospace, Energy Harvesting, Acoustics & Optics*, 9, April 2017, DOI: 10.1007/978-3-319-54735-0_32.

Vuong T-D, Kim K-Y and Dinh C-T (2021) Recirculation-groove coupled casing treatment for a transonic axial compressor, *Aerospace Science and Technology*, Available online 5 February 2021, 106556.

Woodgate MA and Badcock KJ (2009) Implicit Harmonic Balance Solver for Transonic Flow with Forced Motions, *AIAA Journal*, 47(4): 893-901.

Yang Z, Huang R, Liu H, Zhao Y and Hu H (2020) An improved nonlinear reduced-order modelling for transonic aeroelastic systems, *Journal of Fluids and Structures* 94:102926.

Feedback Control of LCOs and Transonic buzz, using the Nonlinear TSD Aerodynamics

Jae Ryong Kwon,

Aerospace Technology Research Institute, Agency for Defense Development,

Daejeon, 34186, Republic of Korea.

Ranjan Vepa,

School of Engineering and Material Science, Queen Mary, University of London,

London, E14NS, UK.

ABSTRACT

In this paper a systematic method to suppress transonic buzz with feedback is presented. A trailing edge control surface in the form of part-span flap was used only to modify and control the unsteady aerodynamic loading on the wing. The flap rotation was used to provide feedback, which consisted of a weighted linear combination of the amplitudes of the principal modes of the structure, referred to as the control law. A linear, optimal feedback control law, that is synthesised systematically based on pseudo-spectral time domain analysis, may be used in principle, to assess its capacity to actively suppress the buzz in the transonic flow domain by using a servo-controlled control surface to modify the unsteady, nonlinear aerodynamic loads on the wing. Thus it is essential that a set of feasible control laws are first constructed. In this paper, this is done by applying the doublet-lattice method (DLM). Restrictions, such as near-zero structural damping in the flap mode, were imposed on the aeroelastic model to facilitate the occurrence of transonic buzz. The feasible set of control laws were then assessed using the nonlinear transonic small disturbance (TSD) theory and an optimum control is selected to suppress the buzz. The essential difference of the behaviour of the closed loop system in non-linear transonic flow, when compared to the applications of linear optimal control in linear potential flow, are presented and discussed.

Keywords: Transonic buzz, Buffeting, Limit cycle oscillator, Feedback control, Transonic small-disturbance theory.

1. Introduction

There are two classes of aeroelastic instabilities driven by aerodynamic non-linearities, which are commonly referred to as buffet and control surface buzz. Oscillations induced in the aircraft lifting or control surfaces due to the presence of a turbulent wake or under the influence of vortex flows are generally referred to as buffeting. Control surface buzz is a sustained aeroelastic oscillation which is a particular type of Limit Cycle Oscillation (LCO) and is observed on trailing edge control surfaces. The continuous interaction of the shocks with a boundary layer especially over a control surface results in the oscillation of the control surface and is known as a buzz. Lambourne (1964) and Bendiksen (1993) provided the earliest classifications of transonic buzz. Rampurawala (2005) has provided an excellent discussion of the existence of buzz in several real aircraft and also considered the prediction of buzz using computation fluid dynamics based analysis techniques. Timme and Badcock (2009) and Woodgate and Badcock (2009) have discussed the application of techniques such the higher order harmonic balance methods to the prediction of transonic buzz. Greco Jr. and Lan (2010) have applied the nonlinear TSD theory to the problem of buzz prediction in the frequency domain rather than in the time domain. Edwards (2010) was able to predict the onset of buffet and the existence of LCOs at transonic speeds. In earlier reviews Dowell and Hall (1996), Dowell, Edwards and Strgnac (2003) and Dowell (2010) have covered the past developments in the prediction of transonic buzz.

The use of high-fidelity methods to obtain the transonic buzz boundaries can be computationally expensive. Considering a typical set of the three-dimensional unsteady Euler equations in conservative differential form and in curvilinear coordinates the state vector is defined by the conservative flow variables vector. The flow variables vector, in its simplest form is at least five dimensional, consisting of the density, flow momentum in three Cartesian directions and the energy. Given the amount of computational time required to perform high-fidelity fluid-structure interaction analyses using the five-dimensional Euler equations over a computational grid spanning the flow field, the model orders are reduced by introducing relevant reduction techniques such as Proper Orthogonal Decomposition (POD) or Polynomial Chaos Expansion. When a reduced order model is adopted, the number of flow variables over the entire flow field are also generally reduced. These computations

must be repeated several times in order to study the oscillatory behaviour under transonic flow conditions. Comparing with the Nonlinear TSD methodology, where one is using only a two-dimensional set of flow variables, the computational cost is reduced substantially, even when reduced order modelling is adopted. Greco Jr. and Lan (2010), Im, Kim and Choi (2018), Shukla and Patil (2017), Howison et al (2018), Taddei (2021), Vuong, Kim and Dinh, (2021), Li and Ekiki (2019), Munk et al (2020), He et al (2019), Prasad (2020) and Prasad and Choi (2020) while Yang et al (2020) used various reduced order models to predict transonic buzz.

Considering the active feedback control of transonic buzz there have been a few attempts to systematically study the effects of feedback on transonic buzz. Verstraelen, Kerschen, Dimitriadis (2017) have attempted to suppress transonic buzz using dynamic vibration absorbers. Marzocca, Silva and Librescu (2002) have alos considered the closed loop analysis of transonic buzz. Goa et al (2017) have considered the analysis of transonic buffet with active controls.

The primary focus of this paper is the suppression of transonic buzz by the use of feedback control. In this paper a systematic, computational model based method to suppress transonic buzz with feedback is presented. There are several unsteady mechanisms in transonic flow, including transonic buzz, pre-buffet flow and transonic buffet onset, forced vibration of aerofoil motion and buffeting response and unstable transonic buffet flow. Although different qualitative interpretation of transonic buzz exist, two conditions must be present for transonic buzz type LCOs to persist. First the linear dynamics of the flap must be in a near state of simple harmonic oscillations. Secondly the nonlinear perturbations to the dynamics due to shock wave motions, boundary layer separation and related transonic phenomenon must be able to sustain the limit cycle oscillations in the single-degree of freedom system. If either of these two conditions are not present, transonic buzz would be inhibited. In this paper, a linear feedback control law is synthesized, so that the first condition is not met. Thus a basic principle for the synthesis of a control law to suppress transonic buzz was established based on the pseudo-spectral time domain analysis of LCOs.

In this paper, furthermore, a trailing edge control surface was used to provide full state feedback. Given a feedback control law, it is possible in principle, to assess its capacity to actively suppress the buzz in the transonic flow domain by using a servo-controlled control surface to modify the unsteady aerodynamic loads on the wing. Thus it is essential that a set of feasible linear control laws are first constructed

by applying the doublet-lattice method (DLM) as was successfully implemented earlier by Vepa and Kwon (2021) for the active suppression of transonic flutter. In this paper the methodology is modified, so the modes of buzz oscillations can be controlled. Restrictions, such as near-zero structural damping in the flap mode, were imposed on the aeroelastic model to facilitate the occurrence of transonic buzz. This aspect is explained in the section 3, after reviewing the analysis of LCOs in section 2. The buzz prediction methodology is discussed in section 4 and the assessment and the selection of an optimum control law to suppress the buzz is considered in section 5. A typical example is considered and the results are presented in sections 6.

2. Analysis of Limit Cycle Oscillators

First the fascinating subject of the analysis of LCOs will be briefly revisited. The Poincaré-Bendixson theorems can be used to identify the presence and absence of limit cycles and establish their uniqueness. These important theorems are explained and are briefly summarized in Vepa (2016). As a result of the Poincaré-Bendixson theorems (see for example Vepa, 2016), in the case of the following second-order equation,

$$\ddot{x} + g(x)\dot{x} + f(x) = 0, \tag{1}$$

where, x is a displacement, $f(x)$ and $g(x)$ are nonlinear functions of x and the dot over the variable $(\dot{x})$ represents differentiation with respect to time t. One may state without proof, that it has a periodic solution which is unique and that this solution is an asymptotically stable orbit under a given set of conditions.

To present the gist of the method of variation of parameters, consider a non-linear system with governing equation of motion expressed as,

$$\ddot{x}(t) + x(t) + \varepsilon F(\dot{x}, x) = 0, \tag{2a}$$

subject to the initial conditions,

$$x(t)\big|_{t=0} = a_0, \ \dot{x}(t)\big|_{t=0} = 0, \tag{2b}$$

where $x(t)$ is the displacement, $F(\dot{x}, x)$ is a non-linear function, ε is a small non-linearity or perturbation parameter and a_0 is a constant. When ε is set equal to zero the solution is of the form,

$$x(t) = a_0 \cos(t + \phi). \tag{3}$$

Hence, when the perturbation parameter ε is not equal to zero the solutions for the displacement and velocity are assumed to be of the form,

$$x(t) = a(t)\cos(t + \phi(t)),\ \dot{x}(t) = -a(t)\sin(t + \phi(t)) \tag{4}$$

where $a(t)$ is a time dependent slowly varying amplitude function and $\phi(t)$ is again a time dependent and slowly varying phase angle, relative to a vector rotating in the phase plane with a constant angular velocity.

Differentiating the assumed solutions and solving for $\dot{a}(t)$ and $\dot{\phi}(t)$, one obtains,

$$\dot{a}(t) = \varepsilon\, F(-a\sin\psi, a\cos\psi)\sin\psi, \tag{5a}$$

$$\dot{\phi}(t) = \varepsilon\, F(-a\sin\psi, a\cos\psi)\cos\psi \tag{5b}$$

where, $\psi = t + \phi(t)$, is the phase angle of the amplitude vector relative to its initial direction. The approximation, known as the *Krylov-Bogoliubov averaging* is introduced by replacing the periodic terms in the right hand sides of the above equations for $\dot{a}(t)$ and $\dot{\phi}(t)$, by their averages over one period of oscillation; i.e. $\psi = 0$ to $\psi = 2\pi$. Further both $a(t)$ and $\phi(t)$ are assumed to be constant over the integration period. Without any loss of generality, the averaged equations take the form,

$$\dot{a}(t) = \varepsilon\, f_{KB}(a),\ \dot{\phi}(t) = \varepsilon\, g_{KB}(a). \tag{6}$$

The response and stability of the slowly varying amplitude function is determined by the first of these averaged equations (6) while the phase angle is the obtained from the second. Orthogonal series expansion in the amplitude and phase plane in terms of ultra-spherical polynomials also leads to equations similar to equations (6).

The method of analysis was first postulated by Denman (1964) and developed by several others. Caughey and Payne (1969) have also considered a similar class of oscillators with stochastic excitation.

Expanding the right hand sides of the equations for the amplitude, $a(t)$ and phase $\phi(t)$ in terms of the variable z, in an orthogonal series of ultra-spherical polynomials with parameter λ and retaining only the first term, one has the approximations,

$$\dot{a}(t) = \varepsilon\, f_U(a, \lambda),\ \dot{\phi}(t) = \varepsilon\, g_U(a, \lambda), \tag{7}$$

as the polynomial, $P_0^{\lambda}(z)$ is a constant. In particular when $\lambda = 1/2$,

$$\dot{a}(t) = \varepsilon\, f_U(a,\lambda)\big|_{\lambda=\frac{1}{2}} = \varepsilon\, f_{KB}(a), \tag{8a}$$

$$\dot{\phi}(t) = \varepsilon\, g_U(a,\lambda)\big|_{\lambda=\frac{1}{2}} = \varepsilon\, g_{KB}(a). \tag{8b}$$

Thus the averaging technique may be interpreted as a generalised orthogonal series expansion based approximation of the equations governing the dynamics in the amplitude and phase plane.

3. Principles of Control Law Synthesis for suppression of LCOs

Following the discussion in the preceding section, to synthesize a controller, since the system behaves like a periodic system as it approaches the limit cycle, and from equations (8), $\dot{a}(t) = \varepsilon\, f_U(a,\ \lambda) \simeq 0$ and $\dot{\phi}(t) = \varepsilon\, g_U(a,\ \lambda) \simeq 0$. Thus it is possible to set, $\varepsilon = 0$ and from equation (5a), one has,

$$\ddot{x}(t) + x(t) + \varepsilon\, F(\dot{x}, x) \simeq \ddot{x}(t) + x(t) \simeq 0. \tag{9}$$

In first order form, with the inclusion of a control input u,

$$\frac{d}{dt}\begin{bmatrix} x \\ \dot{x} \end{bmatrix} = \begin{bmatrix} 0 & 1 \\ -1 & 0 \end{bmatrix}\begin{bmatrix} x \\ \dot{x} \end{bmatrix} + \begin{bmatrix} 0 \\ 1 \end{bmatrix} u. \tag{10}$$

If one wishes to design a steady state feedback regulator that minimizes the performance index,

$$J = \int_0^\infty \left(x^2 + \dot{x}^2\right) dt. \tag{11}$$

An algebraic Riccati equation must be solved and it can be shown that,

$$u = -\begin{bmatrix} k_1 & k_2 \end{bmatrix}\begin{bmatrix} x & \dot{x} \end{bmatrix}^T = -\begin{bmatrix} 0.4142 & 1.3522 \end{bmatrix}\begin{bmatrix} x & \dot{x} \end{bmatrix}^T. \tag{12}$$

The above control input based on the linear-quadratic regulator theory, is independent of $F(\dot{x}, x)$. A simple example will illustrate the open and closed loop responses of a typical oscillator.

The typical example considered is the modified van der Pol equation with parameters $\mathbf{b} = [b_i]$ which may be expressed as,

$$\ddot{x}(t) + x(t) - \left(b_1\left(1 - x^2\right) + b_2\left(1 - \dot{x}^2\right) + b_3\left(1 - x^2 - \dot{x}^2\right) + b_4\left(1 - x^4\right)\right)\dot{x}(t) = u \tag{13}$$

Ignoring the control input, the equations corresponding to (5a) and to (5b) may be respective expressed as,

$$\dot{a}(t) = a(t)\sum_{n=1}^{3} f_{nb}\left(\frac{1-\cos 2n\psi}{2^n}\right),\ \dot{\phi}(t) = \varepsilon\sum_{n=1}^{3} g_{nb}\left(\frac{\sin 2n\psi}{2^n}\right) \tag{14a}$$

where, the functions f_{nb} and g_{nb} may be expressed in terms of amplitude $a(t)$ as,

$$\begin{bmatrix} f_{1b} \\ f_{2b} \\ f_{3b} \end{bmatrix} = \begin{bmatrix} 1 & 1-a^2 & 1-a^2 & 1-a^4/16 \\ -a^2/2 & a^2/2 & 0 & a^4/4 \\ 0 & 0 & 0 & a^4/4 \end{bmatrix} \begin{bmatrix} b_1 \\ b_2 \\ b_3 \\ b_4 \end{bmatrix} \tag{14b}$$

and

$$\begin{bmatrix} g_{1b} \\ g_{2b} \\ g_{3b} \end{bmatrix} = \begin{bmatrix} 1-a^2/2 & 1-a^2/2 & 1-3a^2/2 & 1-5a^4/8 \\ a^2/2 & -a^2/2 & 0 & -a^4 \\ 0 & 0 & 0 & a^4/2 \end{bmatrix} \begin{bmatrix} b_1 \\ b_2 \\ b_3 \\ b_4 \end{bmatrix}. \tag{14c}$$

Expanding $\cos 2n\psi$ and $\sin 2n\psi$ in terms of ultra-spherical polynomials in the interval $[0, 2\pi]$ and retaining only the first term in the orthogonal series expansion, the equations corresponding to equations (7) may be expressed as,

$$\dot{a}(t) = a(t)\sum_{n=1}^{4} b_n f_n(a)\ ,\ \dot{\phi}(t) = 0 \tag{15a}$$

where,

$$\begin{bmatrix} f_1 \\ f_2 \\ f_3 \\ f_4 \end{bmatrix} = \frac{1-U_2}{2}\begin{bmatrix} 1 \\ 1 \\ 1 \\ 1 \end{bmatrix} + \frac{a^2}{8}\begin{bmatrix} 1 & 0 & -1 & 0 \\ 3 & -4 & 1 & 0 \\ 4 & -4 & 0 & 0 \\ 0 & 0 & 0 & 0 \end{bmatrix}\begin{bmatrix} 1 \\ U_2 \\ U_4 \\ U_6 \end{bmatrix} + \frac{a^4}{16}\begin{bmatrix} 0 & 0 & 0 & 0 \\ 0 & 0 & 0 & 0 \\ 0 & 0 & 0 & 0 \\ 2 & 1 & -2 & -1 \end{bmatrix}\begin{bmatrix} 1 \\ U_2 \\ U_4 \\ U_6 \end{bmatrix} \tag{15b}$$

and

$$U_k = \Gamma(\lambda+1)J_\lambda(k\pi)/(k\pi/2)^\lambda\ . \tag{15c}$$

The parameter λ is chosen to be equal to 2 but similar results were obtained for several other choices such that $0 \le \lambda \le 9/2$. The LCO behaviour can be verified by solving equations (15) and plotting the phase-plane trajectory.

A typical set of limit cycle oscillator responses are also generated by simulating equation (13) with the additional control input given by equation (12) and with the parameter set,

$$\mathbf{b} = [0 \quad 0 \quad 0 \quad 1]. \tag{16}$$

The limit cycle responses obtained for the simulated limit cycle oscillator with **b** given by equation (16) and with and without the control input are compared in figure 1. Also shown is the closed loop response for the initially assumed alternate parameter set, **b** given by equation (17),

$$\mathbf{b} = \begin{bmatrix} 1 & 0 & 0 & 0 \end{bmatrix}. \tag{17}$$

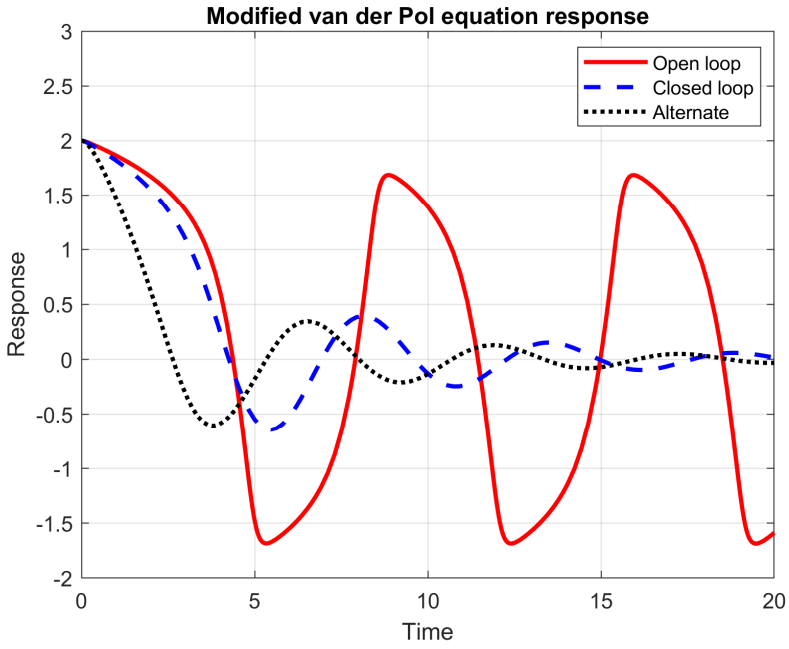

Fig. 1 Comparison of the limit cycle oscillator responses with **b** given by equation (16) and closed loop responses with **b** given by equations (16) and (17).

The principle established in the preceding equations will be applied to the problem of controlling transonic buzz.

4. Prediction of Transonic buzz

In general three-dimensional flow, the unsteady equation for the potential function ϕ, may be written in conservation form as,

$$\frac{\partial f_0}{\partial \tau} + \frac{\partial f_1}{\partial x^*} + \frac{\partial f_2}{\partial y^*} + \frac{\partial f_3}{\partial z^*} = 0, \tag{18}$$

where the functions f_i are functions of the partial derivatives of ϕ given by,

$$f_0 = -M^2\left(\phi_\tau + 2\phi_{x^*}\right), \quad f_1 = \left(1 - M^2\right)\phi_{x^*} + F\phi_{x^*}^2 + G\phi_{y^*}^2, \quad f_2 = \phi_{y^*} + H\phi_{x^*}\phi_{y^*},$$

$$f_3 = \phi_{z^*}. \tag{19}$$

In the equations (19), the coefficients F, G, and H are respectively given by,

$$F=-(\gamma+1)M^2/2,\ G=(\gamma-3)M^2/2,\ H=-(\gamma-1)M^2. \tag{20}$$

where $M=M_\infty$, is the free stream Mach number. Furthermore,

$$x^*=x/c_r,\ y^*=y/c_r,\ z^*=z/c_r,\ \tau=tU_\infty/c_r. \tag{21}$$

There are alternate coefficients that could be used for the coefficients F, G, and H.

	subsonic	supersonic
Far upstream	$\phi=0$	$\phi=0$
Far downstream	$C\phi_t+\phi_x=0$	$\phi_x=0$
Far above	$D\phi_t+\phi_z=0$	$\beta\phi_t+\phi_z=0$
Far below	$D\phi_t-\phi_z=0$	$\beta\phi_t-\phi_z=0$
Far spanwise	$D\phi_t+\phi_y=0$	$\beta\phi_t+\phi_y=0$
Symmetry plane	$\phi_y=0$	$\phi_y=0$

Table I The applicable boundary conditions

The applicable boundary conditions are summarised in Table I. In Table I, the coefficients β, D and C, are given by,

$$\beta=\sqrt{M^2-1},\ D=M\sqrt{1+M^2/(2F\phi_x-\beta^2)},$$
$$C=\left(D\sqrt{(2F\phi_x-\beta^2)}-M^2\right)/(2F\phi_x-\beta^2). \tag{22}$$

The streamwise flux is a major component in the potential equation and is,

$$f_1=(1-M^2)\phi_{x^*}+F\phi_{x^*}^2+G\phi_{y^*}^2. \tag{23}$$

An efficient three-dimensional aerodynamic code based on the nonlinear TSD theory was developed by Batina (1988, 1989, 1992) and later improved by Kim et al (2005) and by Kwon, Yoo and Lee (2018).

Generally, given a reference length such as the root chord c_r, the free stream density ρ_∞ and the free stream flow velocity U_∞, one can construct the generalized aerodynamic forces matrix $\mathbf{Q}$ defined by,

$$\mathbf{Q}=\tfrac{1}{2}\rho_\infty U_\infty^2 c_r^3 \int_{S^*}\left(z_i(x^*,y^*)/c_r\right)\Delta C_{p,j}\left((z_j/c_r),x^*,y^*,M_\infty\right)dS^*, \tag{24}$$

where z_j is the vibration mode shape function of the structure in the j^{th} mode, S^* is the non-dimensional planform area, x^* and y^* are the non-dimensional coordinates of a point in the planform, and M_∞ is the free stream Mach number, the ratio of the free stream flow velocity to the local speed of sound. Furthermore $\Delta C_{p,j}\left(\left(z_j/c_r\right), x^*, y^*, M_\infty\right)$ is the unsteady pressure distribution on the wing surface induced by the j^{th} modal displacement.

The equations of motion of the vibrating wing, including the partial-span trailing edge flap, take the form,

$$\mathbf{M}\ddot{\mathbf{q}} + \mathbf{C}\dot{\mathbf{q}} + \mathbf{K}\mathbf{q} = \mathbf{Q}_{tsd}\left(\mathbf{q},\ \dot{\mathbf{q}}, M_\infty\right) + \mathbf{Q}_{tsd,\eta}\left(\mathbf{q},\ \dot{\mathbf{q}}, M_\infty\right)\eta\,, \tag{25}$$

where the vectors $\mathbf{Q}_{tsd}\left(\mathbf{q},\ \dot{\mathbf{q}}, M_\infty\right)$ and $\mathbf{Q}_{tsd,\eta}\left(\mathbf{q},\ \dot{\mathbf{q}}, M_\infty\right)$ are obtained using a code based on the nonlinear TSD formulation. The integration of the equations (25) is done by a time-marching method, with the appropriate initial conditions as described by Kwon, Kim and Lee (2004) and is the basis of the coupled time integration method (CTIM). In the frequency domain, with all the initial conditions set to zero, a pulse input is used to generate the response as in the transient pulse method (PM), described by Kwon, Kim and Lee (2004).

5. Control Law Synthesis for the Suppression of Transonic Buzz

In the equation (24) for the generalized aerodynamic forces matrix, the integration is performed over the planform area. The modal displacements and slopes at the sending and receiving points in the Doublet Lattice Method (DLM) code are obtained by spline interpolation of the modal displacements at nodes of the structural model. The matrix $\mathbf{Q} = \mathbf{Q}(k)$ is generally complex and a function of the reduced frequency of oscillation, k. If one assumes a matrix Padé approximant representation, the matrix $\mathbf{Q}(k)$ may approximated as,

$$\mathbf{Q}(k) \cong \mathbf{Q}_0 + ik\mathbf{Q}_1 + \left[\mathbf{I} + ik\mathbf{Q}_p\right]^{-1}\mathbf{Q}_r\,, \tag{26}$$

where $\mathbf{Q}_0$ and $ik\mathbf{Q}_1$ are the steady state and low frequency asymptote that can be computed independently, from the steady state and low frequency asymptotes of the

subsonic kernel function as outlined by Vepa (1977). If one assumes, the augmented poles are relatively fast, which is usually the case, $\mathbf{Q}_p \approx \mathbf{0}$, and,

$$\mathbf{Q}(k) \approx \mathbf{Q}_0 + ik\mathbf{Q}_1 + \mathbf{Q}_r . \tag{27}$$

Generally the matrices $\mathbf{Q}_r$, the residue matrix and $\mathbf{Q}_p$, the matrix related to the poles corresponding to the augmented states, are constructed by matching the matrix $\mathbf{Q}(k)$ to the coefficient matrices in the matrix Padé approximant representation at some low value of the reduced frequency, $k = k_f$ close to the estimated flutter reduced frequency, and assuming k is small, it follows that,

$$\mathbf{Q}_0 + \mathbf{Q}_r \cong \mathrm{Re}\left(\mathbf{Q}(k)\right)\Big|_{k=k_f} = \mathrm{Re}\left(\mathbf{Q}\left(k_f\right)\right). \tag{28}$$

Thus $\mathbf{Q}(k)$, computed by the DLM, may be approximated by the zeroth order matrix Padé approximant and is given by,

$$\mathbf{Q}(k) \cong \mathrm{Re}\left(\mathbf{Q}\left(k_f\right)\right) + ik\mathbf{Q}_1 . \tag{29}$$

Thus given the stiffness matrix $\mathbf{K}$, of the structural system, and choosing a suitable model for the structural damping matrix $\mathbf{g}$ which is assumed to be diagonal matrix, the structural damping matrix is $\mathbf{C} = \mathbf{gK}$. The equations of motion are expressed as,

$$\mathbf{M}\ddot{\mathbf{q}} + \mathbf{C}\dot{\mathbf{q}} + \mathbf{K}\mathbf{q} = \mathrm{Re}\left(\mathbf{Q}\left(k_f\right)\right)\mathbf{q} + \left(c_r/U_\infty\right)\mathbf{Q}_1\dot{\mathbf{q}} \ . \tag{30}$$

or equivalently, with the flap included explicitly as,

$$\mathbf{M}\ddot{\mathbf{q}} + \mathbf{C}\dot{\mathbf{q}} + \mathbf{K}\mathbf{q} = \mathrm{Re}\left(\mathbf{Q}\left(k_f\right)\right)\begin{bmatrix}\mathbf{q} & q_\eta\end{bmatrix}^T + \left(c_r/U_\infty\right)\mathbf{Q}_1\begin{bmatrix}\dot{\mathbf{q}} & \dot{q}_\eta\end{bmatrix}^T,$$

$$\ddot{q}_\eta + 2\zeta_\eta\omega_\eta\dot{q}_\eta + \omega_\eta^2 q_\eta + \mathbf{Q}_{\mathbf{H}\eta}\left(\mathbf{q},\ \dot{\mathbf{q}},\ q_\eta,\ \dot{q}_\eta\right) = \omega_\eta^2\eta_c , \tag{31}$$

where the vector $\mathbf{q}$ does not include the flap degree of freedom, q_η is the amplitude of flap degree of freedom, η_c is the flap actuator command input, ω_η is flap actuator natural frequency, ζ_η is the flap actuator damping ratio and $\mathbf{Q}_{\mathbf{H}\eta}$ is the aerodynamic flap hinge moment. It is assumed that the damping ratio in the flap mode is zero as the

flap is in a state oscillation. The assumption is extremely important for the purpose of the synthesis of the control law.

The equations of motion defined by equations (31) may then be cast in the state space form as,

$$\dot{\mathbf{x}} = \mathbf{A}\mathbf{x} + \mathbf{B}\eta_c . \tag{32}$$

Now it is completely feasible to construct an optimal control law based on the above model formulation, defined by equation (32). The optimal control is assumed to minimize a cost function of the form,

$$J\left(\mathbf{x}(t_0), t_0\right) = \int_{t_0}^{t_f} \left(\mathbf{x}^T \mathbf{Q}_x \mathbf{x} + \mathbf{u}^T r \mathbf{R} \mathbf{u}\right) dt + \mathbf{x}^T\left(t_f\right) \mathbf{Q}_f \mathbf{x}\left(t_f\right), \tag{33}$$

where r is a scalar used to alter the control weighting matrix $\mathbf{R}$ in the formulation of the optimal control law synthesis, $\mathbf{Q}_x$ is the state vector weighting matrix and $\mathbf{Q}_f$ is the weighting matrix for the state vector at the final time $t = t_f$. For the single input case, $\mathbf{R} = 1$. The steady-state control law takes the form,

$$\eta_c = \mathbf{u} = -(1/r)\mathbf{R}^{-1}\mathbf{B}^T \mathbf{P}_\infty \mathbf{x} \equiv -\mathbf{K}_f \mathbf{x}, \ \mathbf{P}_\infty \mathbf{A} + \mathbf{A}^T \mathbf{P}_\infty + \mathbf{Q} - \mathbf{P}_\infty \mathbf{B}\mathbf{R}^{-1}\mathbf{B}^T \mathbf{P}_\infty = \mathbf{0}, \tag{34}$$

where $\mathbf{P}_\infty$ satisfies the above algebraic Riccati equation which is solved using a standard function in MATLAB.

Thus given a range of monotonically increasing free stream Mach numbers $M_{\infty,k}$, $k = 1, 2, \cdots,$ as well as a set values for the relative weighting scaling parameter r, one can construct families of control laws, with differing closed-loop stability characteristics. The parameter *r*, in accordance with optimal control theory, is the ratio maximum magnitude of an element in the state vector to the maximum magnitude of the control input as explained by Vepa and Kwon (2021).

In this paper, the parameter r, provides a single scalar parameter to obtain a large distribution of control laws. Each of the control laws may then be used with the open loop dynamics, reformulated in the transonic domain based on the nonlinear TSD theory, and an optimal solution may be selected.

6. Application Example

The example considered, illustrated in figure 2, is the one considered by Kwon, Kim and Lee (2004). The model properties are summarised in Table II. The aerodynamic grid generated and used to solve for the nonlinear TSD aerodynamics is shown in Figure 3. The first three modes in the dynamic model are the first bending, the first torsion mode and the flap oscillation mode controlled by a servo-actuator, while the remaining are higher order modes.

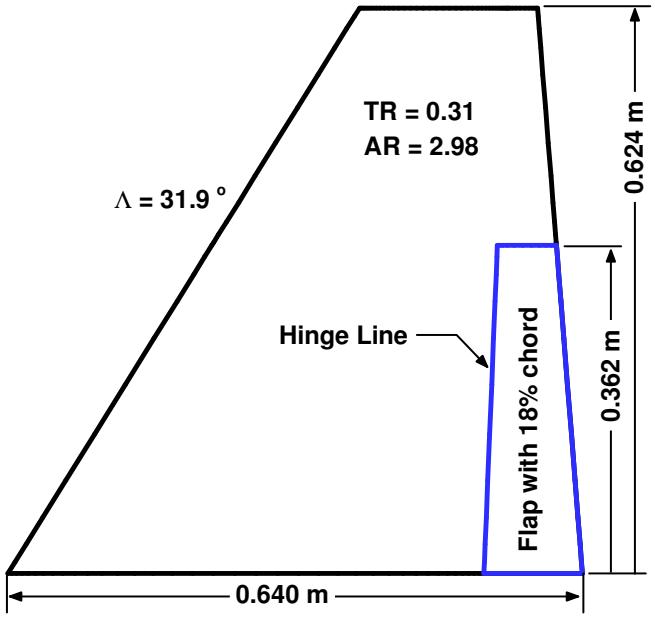

Fig.2 Planform of the application example considered (All dimensions shown are in metres.)

Hinge Stiffness, K_θ	73.4 *Nm/rad*
Flap Moment of Inertia, I_α	0.000842 kgm^2
Material Density, ρ	2770 kg/m^3
Young's Modulus, E	7.31×10^{10} *Pa*
Poisson's ratio, ν	0.33

Table II Model properties.

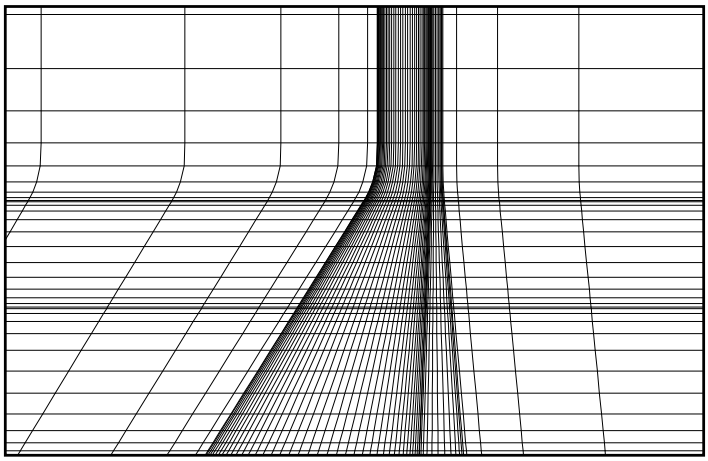

Fig. 3 Aerodynamic grid.

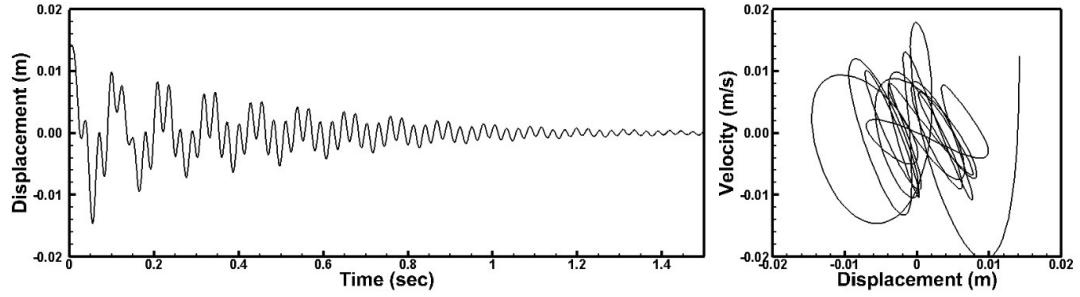

(a)

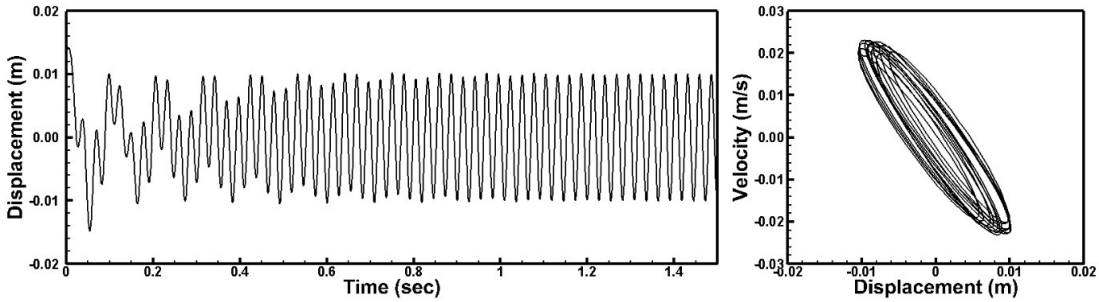

(b)

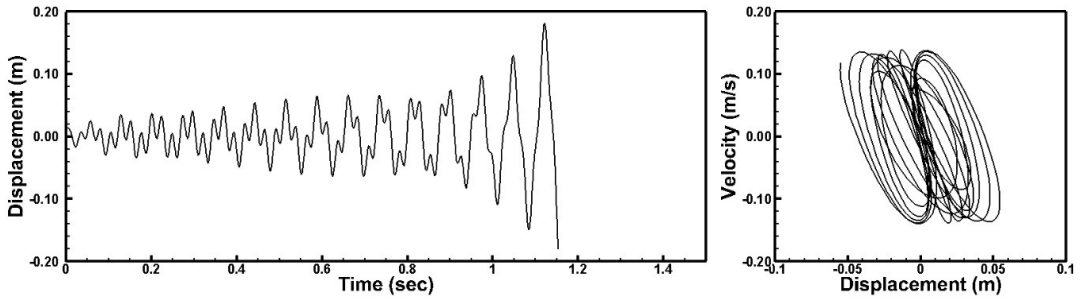

(c)

Fig. 4 Aeroelastic responses at Mach 0.95; (a) 1.49 kPa (Stable), (b) 1.67 kPa (Buzz), (c) 4.83 kPa (Unstable).

7. Typical Simulation Results

In figure 4 are shown the responses of the flap mode at 3 different values of dynamic pressure assuming the flow Mach number far upstream to be $M_\infty = 0.95$. It is seen from figure 4 (b) the response exhibits a transonic buzz type behaviour characterised by sustained periodic oscillations.

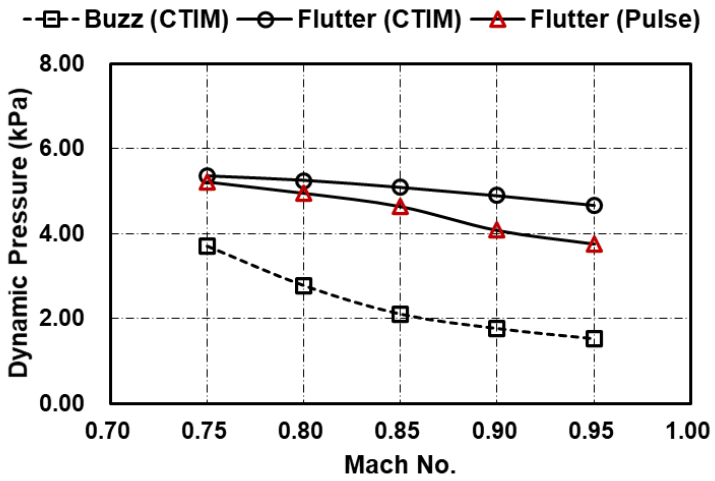

(a)

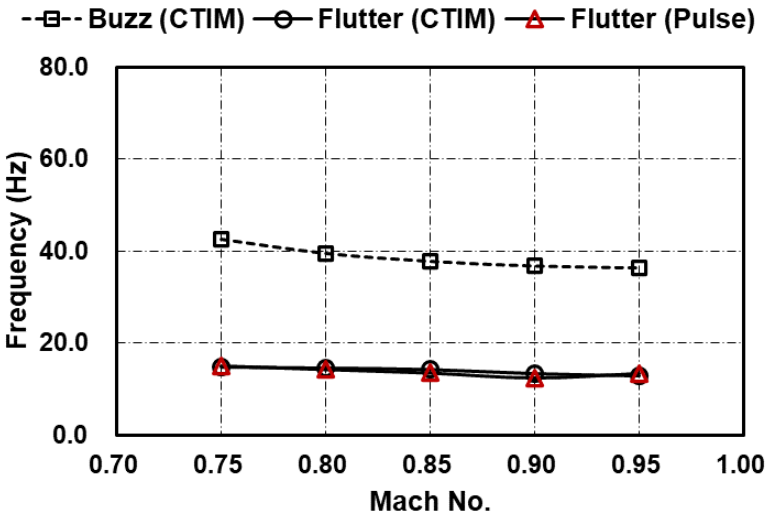

(b)

Fig. 5 Flutter and buzz boundaries with (a) dynamic pressure, (b) frequency versus Mach number.

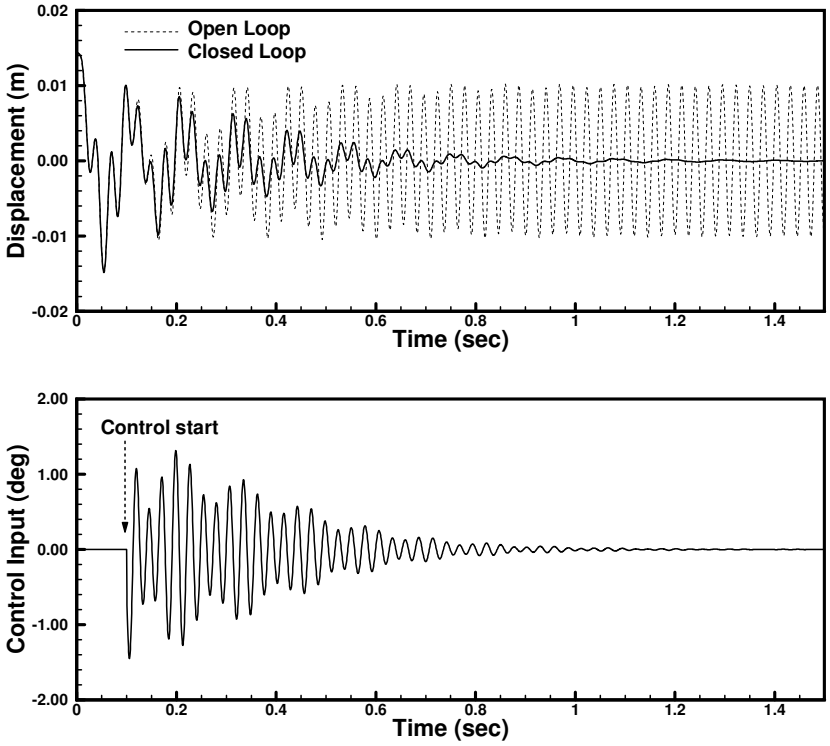

Fig. 6 Typical open and closed loop transonic buzz responses at Mach 0.95 and $q_\infty = 1.67$ kPa as well as the control input time history.

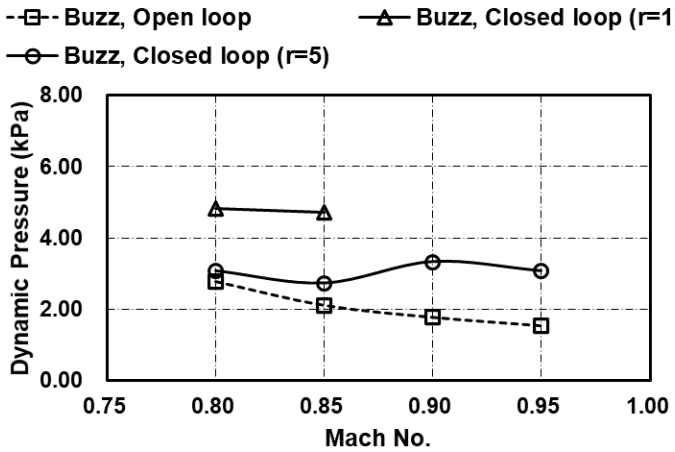

(a)

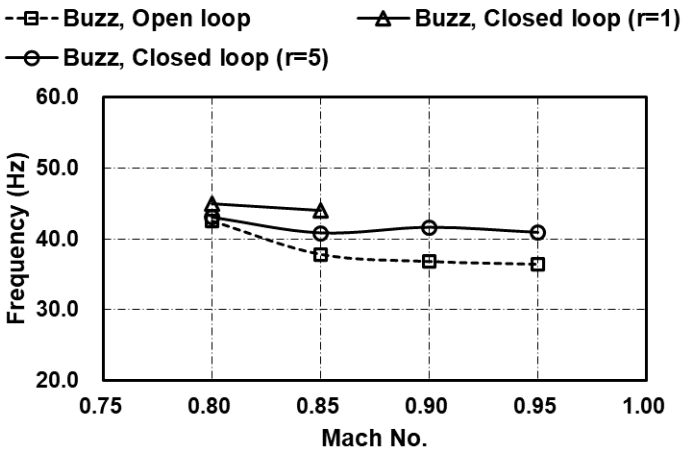

(b)

Fig. 7 Open and closed loop transonic buzz boundaries: (a) dynamic pressures at the boundary and (b) frequencies at the boundary.

The corresponding transonic flutter and buzz boundaries are compared in figure 5. The computations were done by the DLM and the coupled time integration method (CTIM) in the time domain and by the transient pulse method (Pulse) in the frequency domain, for one case, as a check. A single degree of freedom instability associated with the flap mode was observed at a similar set of Mach numbers. These results were used to synthesize the control laws and for r values, in equations (33) and (34), ranging from 1 to 200, in steps of 10 and for 6 different Mach numbers, on the buzz boundary, representing a total of 120 gain vector sets to facilitate a wide search for the optimum set of gains, as explained in sections 3 and 5.

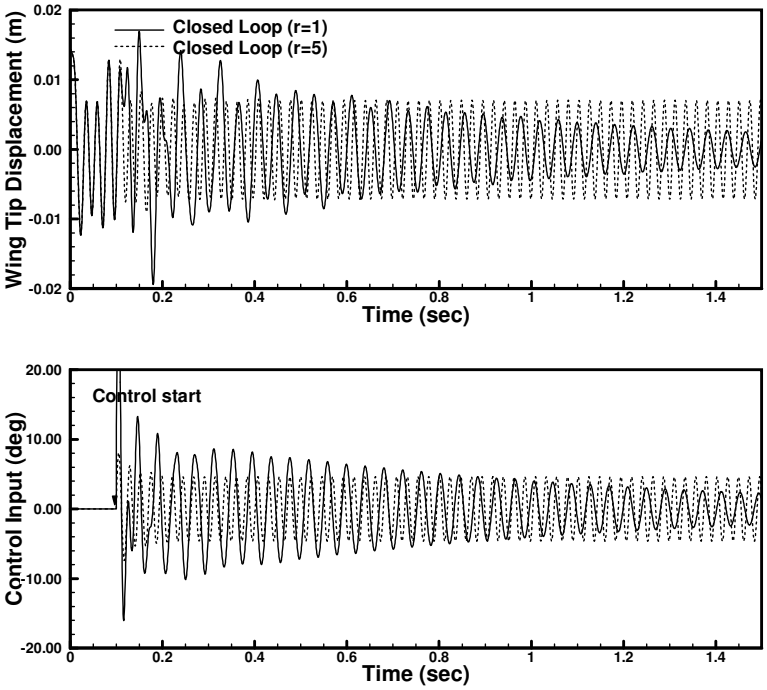

(a) Mach 0.85, $q_\infty = 3.49\,\text{kPa}$

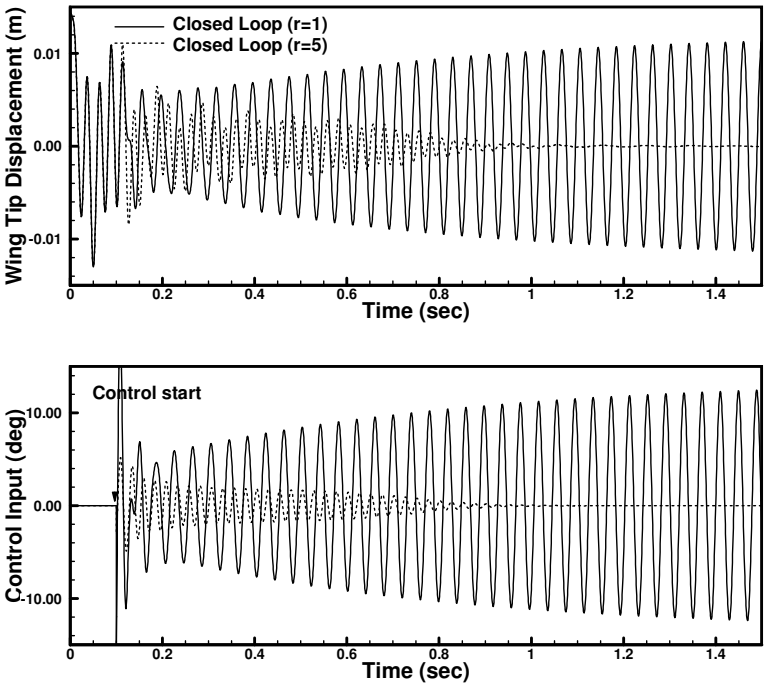

(b) Mach 0.95, $q_\infty = 2.97\,\text{kPa}$

Fig. 8 Transonic buzz control response for $r = 1$ and $r = 5$ (a) Mach 0.85, $q_\infty = 3.49$ kPa and (b) Mach 0.95, $q_\infty = 2.97$ kPa.

The cases in the range of $1 \le r \le 5$, seem to provide the best control laws for maximizing the closed loop buzz velocity or buzz Mach number. In figure 6 are shown a typical set of closed loop transonic buzz responses at Mach 0.95 and $q_\infty = 1.67$ kPa as well as the control input time history. The open loop response is also shown in the background.

In figure 7 are shown a typical set of closed loop transonic buzz boundaries for $r = 1$ and $r = 5$. In the subsonic range below Mach 0.85, r values greater than 1, in the range $1 \le r \le 5$ are effective in suppressing buzz. A summary of the control parameter set applied to the simulation at Mach 0.85, is shown in Table III.

	Control gain set					
r=1	b_1	b_2	b_3	b_4	b_5	b_6
	0.0326	-4.3537	2.3285	-2.7834	0.0000	0.0000
	b_7	b_8	b_9	b_{10}	b_{11}	b_{12}
	-0.0012	0.0244	0.0860	-0.0175	0.0000	0.0000
r=5	b_1	b_2	b_3	b_4	b_5	b_6
	0.0065	-0.8745	0.4676	-0.5586	0.0000	0.0000
	b_7	b_8	b_9	b_{10}	b_{11}	b_{12}
	-0.0002	0.0049	0.0173	-0.0035	0.0000	0.0000

Table III Full state control gain set applied at Mach 0.85

However, in the transonic speed range, such as Mach 0.9 and 0.95, r values much lower than or equal to 1 are not sufficient to suppress buzz. For high Mach numbers, greater than 0.85, the computation of the closed loop buzz boundary at $r = 1$ was quite difficult due to the control surface deflection being too large for these cases, and the closed loop results tend to approach the open loop results. This feature is illustrated in figure 8, for two different r values, $r = 1$ and $r = 5$. The control surface deflection is too large, for r values below $r = 1$. Consequently the optimum range of r values is between $r = 1$ and $r = 5$.

8. Discussion and Concluding Remarks

Quite unlike linear optimal control, there is generally only a finite range of r values, over which the closed loop system is stable with the occurrence of transonic buzz effectively suppressed with reasonable magnitudes of inputs. For higher r values, the magnitude of the control input is insufficient to influence the buzz

behaviour. For lower values of the parameter r, the control inputs are very large and the nonlinear behaviour of the transonic loads is accentuated. In the subsonic range of Mach numbers, below about Mach 0.85, a small value of r is effective in suppressing the buzz. However, in the transonic range of Mach numbers, a value of r equal to or less than one is in-effective in suppressing buzz. This is because the smaller the value of r, the greater the displacement of the control surface, and the unsteady aerodynamics and consequently the wing response is sensitive to the larger displacement of the control surface in the transonic range. The small range of values of r for which the closed loop is stable, implies that for certain configurations, it may be quite impossible for the transonic buzz to be suppressed unless the control surface is designed and optimized specifically for the purpose of suppressing the transonic buzz. Control laws for suppressing transonic buzz must be selected to avoid both low and high magnitudes of control surface deflections. This is the principal contribution of this paper, apart from demonstrating the feasibility of suppressing the occurrence of transonic buzz, by the use of feedback.

Acknowledgements

The authors gratefully acknowledge the support provided by Agency for Defence Development, South Korea, through the award of a Post-Doctoral fellowship to the first author while at Queen Mary, University of London, UK, as part of the Commissioned Continuing Education programme (2019-personnel appointments (Ga)-110).

References

Batina JT (1988) Efficient algorithm for solution of the unsteady transonic small-disturbance equation. *J. of Aircraft* 25(10):962–968

Batina JT (1989) Unsteady transonic algorithm improvement for realistic aircraft applications. *J. of Aircraft* 26(2):131–139.

Batina JT (1992) A Finite-Difference Approximate-Factorization Algorithm for Solution of the Unsteady Transonic Small-Disturbance Equation, NASA Technical Paper 3129, NASA-TP-3129, 19940028359.

Bendiksen O (1993) Non-classical Aileron Buzz in Transonic Flow. 34th AIAA/ASME/ASCE/AHS/ASC Structures, Structural Dynamics and Materials Conference, AIAA paper 93–1479.

Caughey TK and Payne HJ (1967) On the response of a class of self-excited oscillators to stochastic excitation, *Int. J. Non-Linear Mech*. 2:125-151.

Denman, HH (1964) Application of Ultra-spherical Polynomials to Asymmetric Non-linear Oscillations, *J. Industrial Math. Soc*., 14(1):9-20.

Dowell EH (2010) Some recent advances in nonlinear aeroelasticity: fluid-structure interaction in the 21st century. Proceedings of the 51st AIAA/ ASME/ ASCE/ AHS/ ASC Structures, AIAA Paper no. 3137.

Dowell, EH, Edwards JW and Strganac. TW (2003) Nonlinear aeroelasticity. *Journal of Aircraft*, 40(5):857–874, ISSN 0021-8669. doi: 10.2514/2.6876. URL https://doi.org/10.2514/2.6876.

Dowell EH and Hall KC (2001) Modeling of Fluid-Structure Interaction, *Annual Reviews of Fluid Mechanics*, 33:445-490.

Edwards JW (1996) Transonic shock oscillations and wing flutter calculated with an interactive boundary layer coupling method. In 349th EUROMECH-Colloquium: Simulation of Fluid-Structure Interaction in Aeronautics, 16 - 19 Sep., 1996. URL https://ntrs.nasa.gov/search.jsp?R=19960054470.

Gao C, Zhang W, Kou J, Liu Y and Ye, Z (2017) Active control of transonic buffet flow, *J. Fluid Mech*. 824:312-351, Cambridge University Press 2017, doi:10.1017/jfm.2017.344

Greco Jr. PC and Lan CTE (2010) Frequency domain unsteady transonic aerodynamics for flutter and limit cycle oscillation prediction, *Journal of the Brazilian Society of Mechanical Sciences and Engineering*, XXXII(5), Special Issue, 434-441.

He S, Johnson E, Mader CA and Martins JRRA (2019) A Coupled Newton–Krylov Time Spectral Solver for Wing Flutter and LCO Prediction, AIAA Aviation Forum, Dallas, TX.

Howison J, Thomas J and Ekici K (2018) Aeroelastic Analysis of a wind turbine blade using the harmonic balance method, *Wind Energy*, 21(4):226-241.

Im, DK, Kim H and Choi S (2018) Mapped Chebyshev Pseudo-Spectral Method for Dynamic Aero-Elastic Problem of Limit Cycle Oscillation, *International Journal of Aeronautics and Space Sciences*, 19:316 - 329.

Kim J, Kwon H, Kim K, Lee I and Han J (2005) Numerical investigation on the aeroelastic instability of a complete aircraft model. *JSME Int. J.* Ser. B., 48(2):212–217.

Kwon H-J, Kim D-H, I. Lee I (2004) Frequency and time domain flutter computations of a wing with oscillating control surface including shock interference effects, *Aerospace Science and Technology* 8:519–532.

Kwon JR, Yoo J-H and Lee I (2018) Effects of Structural Damage and External Stores on Transonic Flutter Stability, *International Journal of Aeronautical and Space Sciences*, 19:636–644, https://doi.org/10.1007/s42405-018-0063-x.

Lambourne N (1964) Control Surface Buzz. Aircraft Research Council R & M, No. 3364.

Li H and Ekici K (2019) Aeroelastic Modelling of the AGARD 445.6 Wing Using the Harmonic-Balance-Based One-Shot Method, *AIAA Journal*, 57(11):4885-4902.

Liu YK (1965) Application of Ultra-spherical Polynomial Approximation to Non-linear Systems with Two Degrees-of-Freedom, Ph.D. dissertation, Wayne State University.

Marzocca P, Silva WA and Librescu, L (2002) Open/Closed-Loop Nonlinear Aeroelasticity for Airfoils via Volterra Series Approach, Conference Paper, 43rd AIAA/ASME/ASCE/AHS/ASC Structures, Structural Dynamics, and Materials Conference, April 2002, (also in *AIAA Journal*, (2004) 42(4):673-686.)

Munk DJ, Dooner D, Best F, Vio GA, Giannelis NF, Murray AJ and Dimitriadis G (2020) Limit cycle oscillations of cantilever rectangular wings designed using topology optimisation, Proceeding of AIAA SciTech 2020 Forum, 6-10 January 2020, Orlando, FL, USA.

Prasad R (2020) Dynamic Aeroelastic Design using Time-Spectral and Coupled Adjoint Method: Flutter/LCO Application, Doctoral dissertation submitted to the Faculty of the Virginia Polytechnic Institute and State University, Blacksburg, Virginia.

Prasad R and S. Choi S (2020) Aerodynamic Shape Optimization for Flutter/LCO based design using Coupled Adjoint, Proceedings of AIAA SciTech 2020 Forum, 6-10 January 2020, Orlando, FL, USA.

Rampurawala, AM (2005) Aeroelastic analysis of aircraft with control surfaces using CFD. PhD thesis. University of Glasgow, 2005, http://theses.gla.ac.uk/5499.

Shukla H and Patil MJ (2017) Controlling Limit Cycle Oscillation Amplitudes in Nonlinear Aeroelastic Systems, *Journal of Aircraft*, 54(5):1921 – 1932.

Taddei SR (2021) A novel blade force approach to two-dimensional mean line simulation of transonic compressor rotating stall, *Aerospace Science and Technology*, 111:106509

Timme S and Badcock KJ (2009) Oscillatory Behaviour of Transonic Aeroelastic Instability Boundaries, *AIAA Journal*, 47(6):1590-1592.

Vepa R (1977) Finite state modelling of aeroelastic system. NASA CR-2779, February 1977.

Vepa R (2016) Linear and Phase Plane Analysis of Stability, Chapter 4, in *Nonlinear Control of Robots and Unmanned Aerial Vehicles: An Integrated Approach*, CRC Press, 152-197. ISBN: 9781498767040.

Vepa R and Kwon JR (2021) Synthesis of an Active Flutter Suppression System in the Transonic Domain using a Computational Model, *The Aeronautical Journal*, To be published, 2021.

Verstraelen E, Kerschen G and Dimitriadis, G (2017) Flutter and limit cycle oscillation suppression using linear and nonlinear tuned vibration absorbers, *Shock & Vibration, Aircraft/Aerospace, Energy Harvesting, Acoustics & Optics*, 9, April 2017, DOI: 10.1007/978-3-319-54735-0_32.

Vuong T-D, Kim K-Y and Dinh C-T (2021) Recirculation-groove coupled casing treatment for a transonic axial compressor, *Aerospace Science and Technology*, Available online 5 February 2021, 106556.

Woodgate MA and Badcock KJ (2009) Implicit Harmonic Balance Solver for Transonic Flow with Forced Motions, *AIAA Journal*, 47(4): 893-901.

Yang Z, Huang R, Liu H, Zhao Y and Hu H (2020) An improved nonlinear reduced-order modelling for transonic aeroelastic systems, *Journal of Fluids and Structures* 94:102926.